UC San Diego
UC San Diego Previously Published Works

Title

The transcription factors SIX3 and VAX1 are required for suprachiasmatic nucleus circadian output and fertility in female mice

Permalink

Journal

ISSN

Authors

Hoffmann, Hanne M
Meadows, Jason D
Breuer, Joseph A
et al.

Publication Date

2021-10-01

DOI

Peer reviewed

The transcription factors SIX3 and VAX1 are required for suprachiasmatic nucleus circadian output and fertility in female mice

Hanne M. Hoffmann[1,2,3], **Jason D. Meadows**[1,2], **Joseph A. Breuer**[1,2], **Alexandra M. Yaw**[3], **Duong Nguyen**[3], **Karen J. Tonsfeldt**[1,2], **Austin Y. Chin**[1,2], **Brooke M. Devries**[3], **Crystal Trang**[1,2], **Haley J. Oosterhouse**[1,2], **Jessica Sora Lee**[1,2], **Jeffrey W. Doser**[7], **Michael R. Gorman**[2,4], **David K. Welsh**[2,5,6], **Pamela L. Mellon**[1,2]

[1]Department of Obstetrics, Gynecology, and Reproductive Sciences and Center for Reproductive Science and Medicine, University of California, San Diego, La Jolla, CA, USA

[2]Center for Circadian Biology, University of California, San Diego, La Jolla, CA, USA

[3]Department of Animal Science and the Reproductive and Developmental Sciences Program, Michigan State University, East Lansing, MI, USA

[4]Department of Psychology, University of California, San Diego, La Jolla, CA, USA

[5]Department of Psychiatry, University of California, San Diego, La Jolla, CA, USA

[6]Veterans Affairs San Diego Healthcare System, San Diego, CA, USA

[7]CANR Statistical Consulting Center, Michigan State University, East Lansing, MI, USA

Abstract

The homeodomain transcription factors sine oculis homeobox 3 (Six3) and ventral anterior homeobox 1 (Vax1) are required for brain development. Their expression in specific brain areas is

---

maintained in adulthood, where their functions are poorly understood. To identify the roles of *Six3* and *Vax1* in neurons, we conditionally deleted each gene using *Synapsin^{cre}*, a promoter targeting maturing neurons, and generated *Six3^{syn}* and *Vax1^{syn}* mice. *Six3^{syn}* and *Vax1^{syn}* females, but not males, had reduced fertility, due to impairment of the luteinizing hormone (LH) surge driving ovulation. In nocturnal rodents, the LH surge requires a precise timing signal from the brain's circadian pacemaker, the suprachiasmatic nucleus (SCN), near the time of activity onset. Indeed, both *Six3^{syn}* and *Vax1^{syn}* females had impaired rhythmic SCN output, which was associated with weakened *Period 2* molecular clock function in both *Six3^{syn}* and *Vax1^{syn}* mice. These impairments were associated with a reduction of the SCN neuropeptide vasoactive intestinal peptide in *Vax1^{syn}* mice and a modest weakening of SCN timekeeping function in both *Six3^{syn}* and *Vax1^{syn}* mice. Changes in SCN function were associated with mistimed peak PER2::LUC expression in the SCN and pituitary in both *Six3^{syn}* and *Vax1^{syn}* females. Interestingly, *Six3^{syn}* ovaries presented reduced sensitivity to LH, causing reduced ovulation during superovulation. In conclusion, we have identified novel roles of the homeodomain transcription factors SIX3 and VAX1 in neurons, where they are required for proper molecular circadian clock function, SCN rhythmic output, and female fertility.

Keywords

1 | INTRODUCTION

In mammals, circadian rhythms are aligned to the time of day through light signaling from the retina to the suprachiasmatic nucleus (SCN), a small bilateral structure localized in the ventral portion of the hypothalamus. The SCN translates phase and daylength information into nervous and hormonal signals that align circadian rhythms in non-SCN brain areas and peripheral tissues (Bedont et al., 2014; Challet, 2015). Disruption of circadian rhythms through mistimed light or genetic manipulation alters SCN output and circadian alignment in the body and is a risk factor for endocrine disorders such as diabetes, obesity, polycystic ovary syndrome, and reduced fertility (Alvarez et al., 2008; Loh et al., 2014; Mahoney, 2010; Moller-Levet et al., 2013; VanDunk et al., 2011). The development of the SCN is a critical step for its function and coordination of circadian rhythms in the body. A handful of transcription factors have been identified as required for SCN development, including the homeodomain-binding transcription factors, LIM homeobox 1 (*Lhx1*) (Bedont et al., 2014), sine oculis-related homeobox 6 (*Six6*) (Clark et al., 2013; Pandolfi, Tonsfeldt, et al., 2019), sine oculis-related homeobox 3 (*Six3*) (VanDunk et al., 2011), and Ventral anterior homeobox 1 (*Vax1*) (Pandolfi, Breuer, et al., 2019). The roles of *Vax1* and *Six3* in the adult SCN remain unknown, although studies suggest that these transcription factors might play an important role in SCN network function through their regulation of SCN neuropeptides, including vasoactive intestinal peptide (VIP) and arginine vasopressin (AVP) (Bedont & Blackshaw, 2015; Pandolfi, Breuer, et al., 2019; VanDunk et al., 2011).

Ablation of the SCN in adulthood produces a total loss of circadian rhythmicity of the whole animal (Moore & Eichler, 1972; Stephan & Zucker, 1972), where fetal SCN grafts can partly restore rhythms of locomotor activity (Lehman et al., 1987; Ralph et al., 1990) but not hormone release (Meyer-Bernstein et al., 1999). This finding suggests that efferent projections from the SCN control endocrine rhythms and may be centrally involved in disorders impacting hormone release patterns, such as subfertility. Indeed, endocrine disorders are commonly associated with circadian rhythm disruption at the behavioral, hormonal, and/or metabolic level (Alvarez et al., 2008; Loh et al., 2014; Mahoney, 2010; VanDunk et al., 2011). Female reproductive function is particularly sensitive to disrupted circadian rhythms, which cause deregulation of the fine-tuned hormonal feedback loop within the hypothalamic–pituitary–gonadal (HPG) axis. The luteinizing hormone (LH) surge promoting ovulation occurs around the time of activity onset in both diurnal and nocturnal species (Meczekalski et al., 2014; Miller et al., 2006; Russo et al., 2015; Smarr et al., 2013). The SCN is believed to time ovulation through AVP neuron projections onto kisspeptin neurons in the anteroventral periventricular nucleus, and VIP neuron projections onto gonadotropin-releasing hormone (GnRH) neurons in the preoptic area, which can both act to promote the LH surge and ovulation under conditions with permissive estrogen levels (Choe et al., 2013; Christian & Moenter, 2008; Piet et al., 2015, 2016; Schafer et al., 2018; Smarr et al., 2013; Vida et al., 2010; Williams et al., 2011; Williams & Kriegsfeld, 2012). Although it is still debated which specific neuronal population(s) within the SCN gate(s) the LH surge (Bittman, 2019; Sen & Hoffmann, 2019; Smarr et al., 2013), it has been established that both AVP and VIP neurons in the SCN are important. At the level of the pituitary, GnRH promotes release from gonadotropes of LH and follicle-stimulating hormone (FSH), two hormones that drive gonadal maturation, gametogenesis, and ovulation (Kumar & Sait, 2011; Kumar et al., 1998; Kumar et al., 1997; Ma et al., 2004).

Here, we identify a novel role of the homeodomain transcription factors SIX3 and VAX1 in the post-developmental brain. We show that both SIX3 and VAX1 regulate molecular clock function, such that the absence of SIX3 or VAX1 causes impaired SCN circadian rhythm generation, leading to circadian misalignment in reproductive tissues and female subfertility due to loss of the circadian-gated LH surge.

2 | MATERIALS AND METHODS

2.1 | Cell culture and transient transfections

NIH3T3 (American Type Culture Collection) cells were cultured in DMEM (Mediatech), containing 10% fetal bovine serum (Gemini Bio), and 1× penicillin–streptomycin (Life Technologies/Invitrogen) in a humidified 5% CO_2 incubator at 37°C. For luciferase assays, NIH3T3 cells were seeded into 24-well plates (Nunc) at 30,000 cells per well. Transient transfections for luciferase assays were performed using PolyJet™ (SignaGen Laboratories, Rockville, MD), following manufacturer's recommendations. NIH3T3 cells were co-transfected as indicated in the figure legends with 150 ng/well luciferase reporter plasmids, as well as 100 ng/well thymidine kinase-β-galactosidase reporter plasmid, which served as an internal control (Hoffmann et al., 2018). The plasmids used were mouse Vip-luciferase (Hatori et al., 2014), rat Avp-luciferase (Shapiro et al., 2000), mouse Per2-

luciferase (pGL6 plasmid obtained from Addgene.org) (Yoo et al., 2004), mouse Vax1/ pCMV6 overexpression plasmid (20 ng/well, Origene Technologies, Rockville, MD), and mouse Six3/psg5 overexpression plasmid (100 ng/well) (Larder et al., 2011). Site directed mutagenesis of the homeodomain binding sites in the mouse Per2-luciferase plasmid was performed using the NEB Q5 site-directed mutagenesis protocol (New England Biolabs Inc.), following manufacturer's instructions. Primers for NEB Q5 site-directed mutagenesis were designed using the NEB base changer (Table 1). To equalize the amount of DNA transfected into cells, we systematically equalized plasmid concentrations by adding the corresponding inactive plasmid backbone. Cells were harvested 24 hr after transfection in lysis buffer [100 mM potassium phosphate (pH 7.8) and 0.2% Triton X-100]. Luciferase values were normalized to β-galactosidase values to control for transfection efficiency. Values were further normalized by expression as fold change compared to pGL3 control plasmid, as indicated in the figure legends. Data represent the mean ± *SEM* of at least three independent experiments done in duplicate or triplicate.

2.2 | Mouse breeding

All animal procedures were performed according to protocols approved by the University of California, San Diego Institutional Animal Care and Use Committee and the Institutional Animal Care and Use Committee of Michigan State University, and conducted in accordance with the Guide for the Care and Use of Laboratory Animals. Mice were maintained on a light/dark cycle of LD12:12 (12 hr light, 12 hr dark). *PER2::LUC* [Tg(Per2-luc)1Jt, JAX#006852]; *Vax1^{flox}* [Vax1$^{tm1c(KOMP)Mbp}$, MGI: 5796178] (Hoffmann et al., 2016), *Six3^{flox}* [Six3^{tm2Gco}, MGI 3693321] (Liu et al., 2006), and Rosa tdTomato (Ai9, RRID:MGI:104735, JAX #007909) were crossed with *Synapsin^{cre}* [B6.Cg-Tg(Syn1-cre)671Jxm/J, JAX #003966]. Genotyping primer sequences were as follows:

Per2F: CAAAGGCACCTCCAACATG, Per2R: AAAGTATTTGCTGGTGTGACTTG;

Vax1wtF: CCAGTAAGAGCCCCTTTGGG, Vax1floxF: GCCGGAACCGAAGTTCCTA;

Vax1R: CGGATAGACCCCTTGGCATC;

CreF: GCATTACCGGTCGTAGCAACGAGTG, CreR: GAACGCTAGAGCCTGTTTTGCACGTTC;

Six3wtF: TTCCCCTCTTTGACTCCTATGGACG, Six3floxF: CGGCCCATGTACAACGCGTATT,

Six3R: CCCCTAGCCTAACCCAAACATTCG;

Rosa tdTomatoF: CTGTTCTGTACGGCATGG, Rosa tdTomatoR: GGCATTAAAGCAGCGTATCC. *Rosa tdTomato*, *Vax1^{flox}*, and *Synapsin^{cre}* mice were kept on a C57BL/6J background, whereas *Six3^{flox}* were on a mixed C57BL/6J/NMRI background (Liu et al., 2006). All mice were screened for germline recombination to eliminate germline recombined mice from the studies. Mice were housed with lights on from 6 a.m. to 6 p.m. and killed by CO_2 or isoflurane (Vet One, Meridian, ID) anesthesia followed by decapitation.

2.3 | Estrous cyclicity and fertility assessment

For the fertility assessment, virgin 8–12-week-old male and female C57BL/6J, Syn^{cre} $Six3^{fl/fl}$, $Six3^{syn}$, $Vax1^{fl/fl}$, and $Vax1^{syn}$ mice were housed with opposite sex control mice (Hoffmann, 2018; Hoffmann et al., 2014). The number of litters and the number of pups per litter were recorded over a period of 4 months, as described previously (Hoffmann, 2018). Estrous cyclicity was monitored by vaginal lavage with 50 μl H_2O daily between zeitgeber time 3 (ZT3, i.e., 3 hr after lights on in the mouse colony) and ZT5 on 12–20-week-old female mice. The lavage solution was dried on a slide and stained with 0.1% methylene blue. Cytology was visually examined and scored in a blinded manner.

2.4 | Pubertal onset

Pubertal onset was established by visual inspection of preputial separation in males and vaginal opening (VO) in females, as described previously (Hoffmann, 2018). Body weight was recorded daily until pubertal onset was observed.

2.5 | Immunohistochemistry and hematoxylin and eosin (H&E) staining

Twelve- to 20-week-old male and female mice were euthanized between ZT4 and ZT7 by isoflurane overdose and decapitated before ovaries and brains were placed in 60% ethanol, 30% formaldehyde, and 10% glacial acetic acid overnight at 4°C. Tissues were washed in 70% ethanol and embedded in paraffin. Tissues from $Vax1^{syn}$ and $Six3^{syn}$ mice were processed using slightly different embedding and processing protocols, which impacted AVP and VIP antibody efficacy (Figure 5). Single immunohistochemistry on 10 μm coronal brain sections and 5 μm ovarian sections embedded in paraffin was performed as previously described (Hoffmann, Larder, et al., 2019). Primary antibodies were rabbit anti-LHRH (GnRH peptide antibody, Immunostar #20075, dilution 1:1,000, RRID:AB_572248); rabbit anti-VIP (Immunostar #20077, 1:1,000, RRID:AB_572270); rabbit anti-luteinizing hormone receptor (LH/CG receptor antibody, 1:1,000 Cameo et al., 2006; Salvador et al., 2001); and mouse anti-AVP-associated neurophysin (dilution 1:1,000; PS41, Harold Gainer, NIH, Bethesda, MD, USA). Sections were incubated in 1:300 secondary anti-rabbit IgG (Vector Laboratories, #BA-1000). Immunohistochemistry for AVP followed a modified protocol incorporating additional steps for "mouse-on-mouse (M.O.M.)" blocking following vendor's recommendations (M.O.M. kit, Vector Laboratories). The specificity of the mouse antibody was confirmed by comparing staining to a validated rabbit anti-AVP antibody (Immunostar #20069, not shown). Secondary antibodies were purchased from Vector laboratories, and colorimetric VIP (purple staining) and DAB (brown staining) assays (Vector laboratories) revealed the primary antibodies. Immunohistochemistry was quantified using the Lionheart (BioTek Lionheart FX Automated Microscope) Gen5 software (version 3.10 BioTek) by an experimenter blind to genotype. The validity of the automatic quantification was confirmed by a second experimenter, who manually quantified three brains (not shown). For the automated quantification, a total of six sections of the SCN, evenly distributed between Bregma −0.22 and −0.58, were analyzed. For AVP neuron numbers the automated Cellular Analysis function "Cell count" was used. To quantify AVP expressing cells, two rectangles each covering the SCN shell area on each hemisphere were used to define the areas of interest. Data are presented as the sum of AVP expressing neurons on the six sections

quantified. To determine VIP staining intensity two rectangles, each covering the SCN core area on each hemisphere were used to define the areas of interest. To quantitate the intensity of the VIP staining, the setting "Object mean" was used. This setting provides the average intensity of all the pixels located inside the defined object area. The average intensity of the six sections is reported in figures. Counts of GnRH neurons were done by manual counting GnRH-expressing cell bodies on all brain sections between Bregma 3.1 and −1.0. All quantification and image analysis were done by an observer blind to genotype.

Synapsin^cre:tdTomato mice were generated to determine the targets of *Synapsin^cre*. Male and female *Synapsin^cre:tdTomato* mice, 6–10 weeks old, were euthanized by CO_2 overdose and brains, pituitary, testes, ovaries, and uteri placed overnight in 4% paraformaldehyde (PFA), sunk in 30% sucrose, and embedded in TissueTek. Brains were sectioned on an Avantik QS12 cryostat at 40 μm and placed in cryoprotectant (30% sucrose, 1% PVP-40, 30% ethylene glycol in 0.1 M phosphate buffer) at −20°C. Before staining, sections were washed overnight in phosphate-buffered saline (PBS). To visualize tdTomato expression alone, free-floating sections were mounted and coverslipped using ProLong Gold antifade reagent (ThermoFisher Scientific). To examine tdTomato expression in GnRH neurons of female mice, free-floating sections were blocked in 5% goat serum in PBS for 1 hr, washed, and then incubated overnight in GnRH antibody (rabbit anti-GnRH, Immunostar #20075, dilution 1:1,000, RRID:AB_572248). Sections were washed in PBS and incubated for 30 min in 1:100 secondary (goat anti-rabbit 488, Invitrogen, RRID:AB_143165). Sections were washed and mounted using ProLong Gold, and visualized at the UCSD Nikon Imaging Center with a Nikon Eclipse Ti2 equipped with Plan Apo 20× 0.75 NA or 40× S Fluor 0.9 NA objectives. Fluorescence was excited using the Light Engine Aura II Light Engine (Lumencor) with LED emission at 395, 470, or 555 nm. Images were collected using a Nikon DS-Qi1 Qi2 camera and NIS Elements 5.12 software. Images were accessed and figures made using ImageJ.

To visualize tdTomato/RFP immunoreactivity, *Synapsin^cre:tdTomato* male and female mice were euthanized by CO_2 overdose and brains placed in formalin solution (60% EtOH, 30% 37% formaldehyde, 10% acetic acid) overnight at 4°C. Brains were processed (Reveal Biosciences) and embedded, and paraffin-mounted sections were sliced in the sagittal plane at 14 μm. Antigen retrieval was performed in citrate buffer in an antigen retriever (Electron Microscopy Sciences). Slides were blocked using Bloxall, and avidin/biotin blocking in 5% goat serum (Vector laboratories) and placed in RFP antibody overnight (rabbit anti-RFP. Rockland 600-401-379, dilution 1:500, RRID:AB_2209751). Sections were washed in PBS and incubated in rabbit anti-biotin (Vector labs, 1:300), followed by the ABC kit and VIP stain (Vector laboratories). Slices were visualized on an EVOS microscope, white balanced and stitched (Preibisch et al., 2009) using ImageJ.

2.6 | Cresyl violet and H&E staining

Cresyl violet and H&E staining in 12–16-week-old male and female brain tissue were performed on 10 μm coronal tissue sections, and on 5 μm gonadal sections (Vector laboratories and Sigma-Aldrich). Histology was examined by an experimenter blind to genotype. To determine SCN size from cresyl violet and H&E images, the automated

Cellular Analysis function "Object area" in the Gen5 software (version 3.10 BioTek) was used. The area of the SCN was evaluated on 6 evenly distributed sections between Bregma −0.22 to −0.58. In the ovary, the numbers of corpora lutea and follicles were counted manually on every second section in a single ovary per mouse. Fiji-Image Software (NIH) was used to enhance contrast. All image manipulations were applied homogenously to the entire image.

2.7 | Quantitative real-time PCR

For RT-qPCR, the hypothalamus was collected from males that were euthanized by CO_2 overdose. Hypothalami were snap frozen on dry ice and stored at −80°C until RNA extraction. Total RNA was extracted using TRIzol (Invitrogen). Genomic DNA was eliminated using the DNA-free kit (Applied Biosystems). cDNA was obtained by reverse transcription of total RNA using an iScript cDNA synthesis kit (Bio-Rad Laboratories). cDNA products were detected using an iQ SYBR Green Supermix (Bio-Rad Laboratories) on a qRT-PCR CFX real-time detection system (Bio-Rad Laboratories). qRT-PCR primers were previously published (Hoffmann et al., 2014; Larder et al., 2011), *Gnrh1F*: ACACTTGGTTGAGTCTTTCCA, *Gnrh1R*: TGGCTTCCTCTTCAATCAGAC; *GapdhF* TGCACCACCAACTGCTTAG; *GapdhR*: GGATGCAGGGATGATGTTC. Data were expressed as fold change using the 2-δδCT method by normalizing *Gnrh1* to *Gapdh* (Livak & Schmittgen, 2001). Data represent mean fold change ± *SEM* from a minimum of three independent mice for each data point.

2.8 | PCR to detect Flox-allele recombination

To detect *Synapsin^cre*-induced *Six3^flox* and *Vax1^flox* allele recombination, females were euthanized with CO_2 overdose between ZT3 and ZT6, and brains snap frozen on dry ice. On a cryostat, 300 μm coronal brain sections were prepared, and bilateral 0.25 mm punches of the: olfactory bulb, nucleus accumbens, piriform cortex, caudate putamen (striatum), cingulate cortex, ventral pallidum, magnocellular preoptic nucleus, supraoptic nucleus, dentate gyrus, hippocampal area CA2, basolateral amygdala, medial amygdala, and ventrolateral thalamic nucleus collected. The paraventricular nucleus was collected with one punch due to the size of the brain area. Genomic DNA was extracted using DNeasy Kit (Qiagen) according to manufacturer's instructions. The following primers were used Six3RecF: CCCCTAGCCTAACCCAAACAT, Six3RecR: TTCCCCTCTTTGACTCCTATG, annealing temperature 59°C. Vax1RecF: GCAGTGGCCTAGAGAGATCG, Vax1RecR: GCACTGTGTAGTGCTCCTAT, annealing temperature 62.5°C. PCR products were separated on a 2% agarose gel.

2.9 | GnRH and kisspeptin challenges, and hormone assays

For GnRH and kisspeptin challenges, tail blood was collected from adult female metestrus/diestrus littermates between ZT4 and ZT6. A first tail blood collection was done prior to the hormone challenge. A second collection of tail blood was performed 10 min after receiving an i.p. injection of 1 μg/kg GnRH in sterile saline, or 10 min (in *Six3^syn*) or 20 min (in *Vax1^syn*) after receiving an i.p. injection of 3 nmoles kisspeptin-10 (Tocris 4243) in sterile saline. For all other serum hormone analyses, mice were killed by isoflurane overdose and blood collected from the abdominal aorta between ZT3 and ZT6. Blood was allowed to

clot for 1 hr at RT, then centrifuged (RT, 15 min, $2,600\times g$). For intratesticular testosterone evaluation, testis was snap frozen on dry-ice. One testis was homogenized in PBS containing protease inhibitors (Sigma) and left at RT O/N. Samples were centrifuged at RT to remove tissue debris. 1:1 dichloromethane was added to the supernatant. Samples were centrifuged (RT, 5 min, $2,300\times g$). Supernatant was mixed 1:1 with dichloromethane, and centrifuged (RT, 10 min, $4,600\times g$). Pellet was collected and resuspended in ELISA buffer (Endocrine technologies, ERL R7016 testosterone). Serum and intratesticular testosterone were collected and stored at $-20°C$ before analysis for estradiol (E2), progesterone (P4), and testosterone (T) at the Center for Research in Reproduction, Ligand Assay, and Analysis Core, University of Virginia (Charlottesville), or by Luminex analysis for LH and FSH on MILLIPLEX MAP Mouse Pituitary Magnetic Bead Panel (Millipore Sigma #MPTMAG-49k). Coefficients of variance (CVs) were based on the variance of samples in the standard curve run in duplicate or triplicate. Reportable range: P4: 0.15–20 ng/ml, CV = <20%; E2: 3–300 pg/ml, CV = <20%; T: lower detection limit: 9.6 ng/dl, CV < 10%; LH: lower detection limit: 5.6 pg/ml, CV < 15%; FSH: lower detection limit: 25.3 pg/ml, CV < 15%. Samples were run in singlets.

2.10 | Ovariectomy and estrogen replacement

To study the LH surge around activity onset, we used the validated ovariectomy + estradiol implant surge model modified from (Bronson & Vom Saal, 1979). Adult female mice (8–16 weeks of age) were anesthetized by isoflurane inhalation, ovariectomized, and implanted subcutaneously in a mid-scapular location with estrogen capsules (1 cm length). The silastic capsules contained a mixture of 1.2 mg β-estradiol (E8875; Sigma Aldrich) in 4 ml silastic silicone adhesive (3244393; Dow Corning Corp.) with an inner diameter of 1.02 mm and outer diameter 2.16 mm (508005; Dow Corning Corp.) giving each mouse 2.5 ng β-estradiol. The estrogen capsules were placed in PBS at 4°C the day before surgery to ensure proper estrogen transport across the tubing membrane. Post-operative care included at least two buprenorphine HCl injections (Reckitt Benckiser) of 0.1 mg/kg body weight just after surgery and 12 hr later for pain management. One and two weeks, later the ovariectomized, estrogen-treated females were injected subcutaneously with 1 μg estradiol benzoate (E8515; Sigma Aldrich) in 100 μl sesame seed oil. All injections occurred between ZT3 and ZT4. The next day, tail blood was collected at ZT4 to assess basal LH in the morning, whereas trunk blood was collected at ZT12.5 to detect whether the endogenous LH surge occurred. Trunk blood was collected after CO_2 inhalation and euthanasia.

2.11 | Oocyte release in response to ovarian stimulation

Ovulation was induced using a combination of pregnant mare serum gonadotropin (PMSG) and human chorionic gonadotropin (hCG). Female mice at 10 weeks of age were hormone primed with an *i.p.* injection of 5 IU of PMSG (G4877, Sigma-Aldrich) applied at ZT12 and ovulation was induced 48 hr later by an *i.p.* injection of 5 IU of hCG (Novarel, Ferring Pharmaceuticals, Parsippany, NJ). On the morning following the hCG injection, mice were sacrificed at ZT12. Each oviduct was carefully examined for released oocytes by making a small incision in the oviduct and gently expelling the content of the entire oviduct. The cumulus mass was dissociated by treatment in Hank's Balanced Salt Solution

(HBSS) containing 300 μg/ml hyaluronidase (Sigma-Aldrich, St Louis, MO), for counting the oocytes. Oocytes were distinguished from other detritus by their spherical nature.

2.12 | Wheel-running behavior

At age 8–12 weeks, females were single housed in cages containing running wheels with magnets, and wheel revolutions were monitored using magnetic sensors. All cages were contained in a light-tight cabinet with programmable lighting conditions and monitored for temperature and humidity. Food and water were available ad libitum during the entire experiment. After 1-week acclimation to the polypropylene cages ($17.8 \times 25.4 \times 15.2$ cm) containing a metal running wheel (11.4 cm diameter), locomotor activity rhythms were monitored with a VitalView data collection system (Version 4.2, Minimitter, Bend OR) that integrated in 6 min bins the number of magnetic switch closures triggered by half wheel rotations. Running wheel activity was initially monitored for 2 weeks in a standard light/dark cycle of 12 hr light, 12 hr dark (LD 12:12). Subsequently, mice were monitored for 4 weeks in constant darkness (DD), with wheel-running data analyzed from weeks 2–4 in DD. Cage changes were scheduled at 3-week intervals. Wheel-running activity was analyzed using ClockLab Analysis (ActiMetrics) by an experimenter blind to experimental group. Circadian period was analyzed by constructing a ClockLab-generated least-squares regression line through a minimum of 13 daily activity onsets. Daily onset and offset of activity, defined as a period of 5 hr of activity following 5 hr of inactivity (onset) or a period of 5 hr of inactivity following 5 hr of activity (offset), were used to calculate the length of the active phase (alpha). χ^2 periodograms (Sokolove & Bushell, 1978) were generated for periods from 0 to 36 hr, with significance set at 0.001. Any mice that did not exhibit a significant peak between 18 and 36 hr were deemed arrhythmic and were not included in analyses, and the maximum amplitude was reported as Qp. Activity profiles were generated for weeks 2–4 in DD using the circadian period (tau) estimated from the χ^2 periodogram for the same time interval. Total daily counts were calculated over 24 hr, during both LD and DD.

2.13 | Ex vivo tissue recordings of PER2::LUC expression

For SCN, pituitary, and ovary explant studies, female PER2::LUC circadian reporter mice were used, in which the endogenous *Per2* gene was replaced by homologous recombination with a fusion of mouse *Per2* and firefly *luciferase* genes, incorporating all transcriptional and post-transcriptional regulatory elements to allow robust rhythmic expression of the PER2::LUC fusion protein (Yoo et al., 2004). Diestrus PER2::LUC females were sacrificed at ZT3-4 via isoflurane inhalation and cervical dislocation. The pituitary, ovary, and brain were removed immediately and placed in ice-cold HBSS for approximately 30–60 min. Using a Vibratome (Leica), coronal brain sections of 300 μm were collected, and the SCN was dissected from the slices in ~2×2 mm squares. An SCN, one ovary, or one pituitary was placed individually on a 30 mm Millicell membrane (Millipore-Sigma) in a 35 mm cell culture plate containing 1 ml Neurobasal-A Medium (Gibco) with 1% Glutamax (Gibco), B27 supplement (2%; 12349-015, Gibco), and 1 mM luciferin (BD Biosciences). The lid was sealed to the plate using vacuum grease to ensure an air-tight seal. Plated tissues were loaded into a LumiCycle luminometer (Actimetrics) inside a 35°C non-humidified incubator at ZT6-6.5, and recordings were started. The bioluminescence was counted for 70 s every

10 min for 6 days (day 1–day 7 of recording time). PER2::LUC rhythm data were analyzed using LumiCycle Analysis software (Actimetrics) by an experimenter blind to experimental group. Data were detrended by subtraction of the 24 hr running average, smoothed with a 2 hr running average, and fitted to a damped sine wave (LM Fit, damped). Phase was then defined as the time of the first peak of the fitted curve. Period was defined as the time in hours between the peaks of the fitted curve. Peaks were defined as points at which the bioluminescence was higher than at adjacent points. Amplitude was defined as the amplitude of the fitted sine wave (Shinozaki et al., 2017).

2.14 | Statistical analysis

Statistical analyses were performed with GraphPad Prism 8, using Student's t test, one-way ANOVA or two-way ANOVA, followed by post hoc analysis by Tukey or Bonferroni as indicated in figure legends, with $p < 0.05$ to indicate significance. GnRH neurons are not known to be sexually dimorphic, so data from males and females were combined for GnRH neuron counts. PER2::LUC timing of first peak phase relationships was analyzed in R via a Circular Analysis of Variance High Concentration F-Test, with a corrected confidence level of $p < 0.01667$ to account for family-wise error. Wheel-running activity was analyzed via a two-way repeated measures ANOVA. To estimate the number of animals required to reach a power of 0.7, we used GPower to estimate group size (n per group) using a one-way ANOVA, fixed effect size. Based on preliminary data, we expected to see a modest-to-strong impact of *Six3* and *Vax1* conditional KO on the analyzed parameters. With $a = 0.3$, an effect size $= 0.4$ and a study power of 0.7, each individual group requires $n = 8$ mice. Thus, the power of most of the data reported in this study is ~0.6–0.7.

3 | RESULTS

3.1 | SIX3 and VAX1 are required for normal fertility in adult female mice, but not in males

Six3 is broadly expressed in the postnatal day 4 (P4) mouse brain (https://developingmouse.brain-map.org/experiment/show/100056626), whereas *Vax1* is primarily expressed in parts of the olfactory bulb and hypothalamus (Figure 1a, https://developingmouse.brain-map.org/experiment/show/100078609). Both *Six3* and *Vax1* retain expression in the adult brain, where *Six3* is expressed throughout the brain, with high expression in the olfactory bulb and the suprachiasmatic nucleus (SCN) of the hypothalamus Figure 1a, P56. https://developingmouse.brain-map.org/experiment/show/81654113). In contrast, *Vax1* expression is very limited at P56, detected primarily in the SCN (Figure 1a, P56, https://developingmouse.brain-map.org/experiment/show/81655570). To understand the roles of *Six3* and *Vax1* after neuronal maturation, we crossed *Six3^fl/fl* and *Vax1^fl/fl* mice with *Synapsin^cre* mice, herein referred to as *Six3^syn* and *Vax1^syn*. *Synapsin^cre* targets expression of Cre recombinase specifically to maturing and mature neurons (Mori et al., 2004; Zhu et al., 2001). *Synapsin^cre* mice were crossed with Rosa tdTomato mice to visualize where *Syn^cre* was active (*Synapsin^cre:tdTomato*). We found that *Syn^cre*, as indicated by tdTomato (Figure 1bi) or RFP (Figure 1bii), was abundant in the adult SCN. Overall, tdTomato/RFP was widely expressed in the brain, particularly in the cortex and hippocampus (Figure 1biii). We observed more limited expression pattern in the hypothalamus, including the SCN, dorsomedial hypothalamus, and ventromedial hypothalamus. In addition, we found

Synapsyn^cre-driven tdTomato expression in some cells of the pituitary, ovary, and uterus, (Figure 1c), consistent with known frequent germline recombination when breeding through *Synapsin^cre* (Rempe et al., 2006). No recombination was detected in the testis (Figure 1c). Next, to evaluate recombination of the *Six3^fl/fl* and *Vax1^fl/fl* alleles by *Synapsin^cre*, we performed PCR for *Six3^fl/fl* and *Vax1^fl/fl* recombination. We found that *Synapsin^cre* recombined the *Six3^fl/fl* and *Vax1^fl/fl* alleles in all of the studied brain areas, including the adult hypothalamus, SCN, cortex, olfactory bulb, paraventricular nucleus, medial amygdala, nucleus accumbens, and suprachiasmatic nucleus (Figure 1d). The extensive overlap of *Six3* and *Vax1* (Figure 1a) with *Synapsin^cre* in the hypothalamus, led us to focus on physiological functions regulated by the hypothalamus, one of which is reproduction.

To determine whether the absence of SIX3 or VAX1 in adult neurons affects reproductive function, we performed a 4-month fertility assay. We found that both *Six3^syn* and *Vax1^syn* females, but not males, were sub-fertile to infertile (Figure 2a,b). The impaired fertility of *Six3^syn* and *Vax1^syn* females was not due to lack of pubertal onset, as established through vaginal opening in females and preputial separation in males. In *Six3^syn* females, vaginal opening occurred at a later age but upon reaching a similar body weight to controls (Table 2), whereas preputial separation in males happened at a comparable age in *Six3^syn* and control mice (Table 2). In *Vax1^syn* mice, vaginal opening and preputial separation were not significantly impacted compared to controls (Table 3). Both *Six3^syn* (Table 2) and *Vax1^syn* (Table 3) males had normal testosterone levels. As male fertility was intact overall, we focused the remaining studies on understanding the origin of the reduction in female fertility.

Hormone feedback mechanisms involving the hypothalamus, pituitary, and ovary allow proper progression of the estrous cycle. Both *Six3^syn* and *Vax1^syn* females presented irregular and prolonged estrous cycles [Figure 2c (estrous cycle length: *Six3^syn* $p = 0.046$, $n = 8$), and Figure 2d (*Vax1^syn* $p = 0.006$, $n = 9$)], although time spent in each estrous stage was unaffected (Figure 2e,f). The irregularity in estrous cyclicity did not impact estradiol levels to a detectable degree during diestrus (estradiol levels were below detection limit, $n = 5$–10, not shown), nor was it associated with abnormal numbers of corpora lutea, progesterone-secreting structures within the ovaries that develop after ovulation [Figure 2g,h; number of corpora lutea (CL), t test, $p < 0.05$]. The irregular estrous cycles suggest abnormal pituitary hormone release. Basal LH levels were significantly increased in diestrus *Six3^syn* females, without impacting FSH levels (Table 2), whereas LH and FSH levels in *Vax1^syn* females were comparable to controls (Table 3). The modest increase in LH in the *Six3^syn* females is unlikely to be sufficient to account for their marked subfertility, so we focused further studies on hypothalamic GnRH neurons.

Female fertility requires coordinated high estrogen and SCN input to hypothalamic kisspeptin and GnRH neurons, allowing a surge of LH around activity onset. We have previously shown that early developmental deletion of *Six3* causes abnormal GnRH neuron migration and increases the total number of GnRH neurons, which does not impact fertility, whereas early developmental deletion of *Vax1* in GnRH neurons abolishes GnRH expression, causing infertility (Hoffmann et al., 2016; Pandolfi et al., 2018). GnRH neurons are not thought to be sexually dimorphic, and developmental manipulations

impact GnRH neuron numbers to a similar degree in both males and females. To determine if the *Synapsin^cre* allele targets GnRH neurons in adult mice, we performed dual immunohistochemistry in *Synapsin^cre:tdTomato* mice for GnRH and tdTomato (marking cells targeted by the *Synapsin^cre* allele). In 147 GnRH neurons counted from three adult female animals (14–74 neurons/animal), only two showed colocalization with tdTomato (Figure 2i). Despite this low rate of targeting of GnRH neurons by the *Synapsin^cre* allele, GnRH immunohistochemistry in *Vax1^syn* mice revealed a >twofold increase in the number of GnRH neurons relative to control mice (Figure 2j,k). Based on our previous work showing that loss of *Six3* had a minor effect on GnRH neuron numbers, which did not directly impact fertility (Pandolfi et al., 2018), and the capacity of qPCR to correctly reflect changes in *Gnrh1* mRNA expression (Hoffmann et al., 2014), we decided to evaluate *Gnrh1* expression levels in *Six3^syn* mice with qPCR instead of immunohistochemistry. As expected, we found that *Six3^syn* mice exhibited levels of hypothalamic *Gnrh1* expression comparable to those of controls (Figure 2I), supporting the differential roles of *Six3* and *Vax1* in GnRH neuron development (Hoffmann et al., 2016; Pandolfi et al., 2018). To determine if the increase in number of GnRH neurons in *Vax1^syn* mice impacted the LH surge, we first confirmed that *Six3^syn* and *Vax1^syn* pituitary responded correctly to a GnRH challenge by releasing LH (Figure 2m, *t* test, $p > 0.05$), and next tested GnRH neuron sensitivity to kisspeptin. The kisspeptin challenge elicited an increase in LH in all the mice studied (Figure 2n), showing that GnRH neurons can produce an LH surge from the pituitary in both of our conditional KO mouse lines. However, despite the intact sensitivity of GnRH neurons to kisspeptin, and normal pituitary sensitivity to GnRH, neither *Six3^syn* nor *Vax1^syn* females presented the expected LH surge at activity onset in an estrogen-induced surge model (Figure 2o). We therefore moved on to explore circadian gating of the LH surge as a possible cause of subfertility in these two mouse models.

3.2 | *Six3^syn* and *Vax1^syn* mice have altered SCN circadian locomotor activity rhythm output

To determine if SCN function was impacted in female *Six3^syn* and *Vax1^syn* mice, we assessed wheel-running patterns in a standard 12:12 light–dark cycle (LD) and in constant darkness (DD), allowing examination of both entrainment to the light–dark cycle and endogenous free-running rhythms. One *Six3^fl/fl* female was arrhythmic in DD and was not included in the analyses. Female *Six3^fl/fl* ($n = 8$) and *Six3^syn* ($n = 13$) mice (Table 4, Figure 3a) entrained normally to LD, with a 24 hr period (Figure 3b), and had comparable alpha to controls (Figure 3c). In DD, both *Six3^syn* and *Six3^fl/fl* females had shorter periods than in LD [$F(1,19) = 7.93$; $p = 0.01$], reflecting endogenous free-running rhythms, with no differences in period length or alpha between genotypes. It should be noted that in addition to an overall shortening of free-running circadian period (Tau) in *Six3^syn* females, there was also a large variability, ranging 23.1–24.7 hr (Figure 3b). This higher variability in Tau is consistent with the significantly weaker circadian rhythms found in *Six3^syn* as compared to *Six3^fl/fl* mice (Figure 3d,e). The weakening of circadian rhythms was further supported by the reduced rhythm amplitude, indicated by the lower peak value of the DD activity profile in *Six3^syn* compared to *Six3^fl/fl* mice (Figure 3f). The impact on wheel-running behavior was less severe in *Vax1^syn* mice (Table 5, Figure 4). Female *Vax1^syn* ($n = 7$) mice (Figure 4a) exhibited an intact circadian phenotype, with period and alpha comparable to *Vax1^fl/fl*

mice (n = 10) under both LD12:12 and DD (Figure 4b,c). Rhythm strength of *Vax1^{syn}* and *Vax1$^{fl/fl}$* females was similar in LD. In DD, *Vax1^{syn}* mice displayed significantly weaker circadian rhythms compared to controls (Figure 4d,e), but there were no significant differences in DD activity profile amplitude between *Vax1^{syn}* and *Vax1$^{fl/fl}$* mice (Figure 4f).

3.3 | SIX3 and VAX1 alter adult SCN neuropeptide expression

SCN neurons containing the neuropeptides AVP and VIP send projections to hypothalamic kisspeptin and GnRH neurons, respectively (Horvath et al., 1998; van der Beek et al., 1997; Vida et al., 2010; Williams et al., 2011). AVP and VIP have been shown to alter the timing of the LH surge (Palm et al., 1999), and firing of kisspeptin (Piet et al., 2015) and GnRH neurons (Christian & Moenter, 2008; Piet et al., 2016). Thus, SCN AVP and VIP projections likely modulate LH release from the pituitary through GnRH and kisspeptin neurons. Evaluation of SCN morphology and size by hematoxylin/eosin staining (H&E or Cresyl Violet) showed comparable SCN size across groups (Figure 5a–d). To assess whether AVP and VIP peptide expression was impacted in *Six3^{syn}* or *Vax1^{syn}* mice, we performed VIP and AVP immunohistochemistry. We found that in *Six3^{syn}* mice, VIP peptide (Figure 5e,f) and AVP peptide expression (Figure 5i,j) were comparable to controls. In contrast, *Vax1^{syn}* mice had less VIP expression than controls (Figure 5g,h), and fewer AVP expressing cells than controls (Figure 5k,l). To determine if SIX3 and VAX1 might regulate *Vip* or *Avp* transcription *in vitro*, we transiently transfected NIH3T3 cells with a *Vip* (Figure 5m) or *Avp* (Figure 5n) promoter driving luciferase expression. *In vitro*, SIX3 did not regulate *Vip-luciferase* expression, but strongly enhanced *Avp-luciferase* expression (Figure 5m,n). In contrast, VAX1 significantly enhanced *Vip-luciferase* expression, but did not regulate *Avp-luciferase* expression (Figure 5m,n).

3.4 | SIX3 and VAX1 regulate expression of the clock gene *Per2* and alter SCN circadian period

The modest (*Vax1^{syn}*) or undetectable (*Six3^{syn}*) impact on AVP and VIP expression in the conditional KO mice (Figure 5e–l) cannot fully explain their reduction in female fertility (Figure 2a,b) or impaired wheel-running patterns in DD (Figures 3 and 4). As transcription factors, SIX3 and VAX1 could regulate expression of several circadian clock genes with ATTA or ATTA-like sites in their regulatory regions. The molecular circadian clock includes numerous transcription factors that are necessary for generation of an autonomous ~24 hr rhythm within cells. Altered expression, localization, or function of clock gene products can disrupt the ~24 hr rhythm of the molecular clock (Liu et al., 2007; Welsh et al., 2004, 2010; Yoo et al., 2004), resulting in abnormal wheel running (Reppert & Weaver, 2002).

We found that the *Per2* regulatory region contains numerous ATTA and ATTA-like binding sites, sites known to be bound by SIX3 and VAX1 (Table 1). Therefore, we transiently transfected the *Per2-luciferase* reporter plasmid into NIH3T3 cells with and without SIX3 and VAX1. Both SIX3 and VAX1 enhanced expression of the *Per2-luciferase* plasmid containing the proximal promoter, exon 1, and intron 1 of *Per2* (−1,128 bp to +2,129 bp from the transcriptional start site, Figure 6a,b). A two-way ANOVA showed an overall effect of SIX3 on *Per2-luciferase* expression [$F_{(1,27)}$ = 207.8, $p < 0.0001$] and an overall effect of VAX1 on *Per2-luciferase* expression [$F_{(1,29)}$ = 111.1, $p < 0.0001$], as well as an

interaction between *Per2-luciferase* promoter constructs and SIX3 [$F_{(6,27)} = 3.300$, $p = 0.014$] and interaction between *Per2-luciferase* promoter constructs and VAX1 [$F_{(6,29)} = 6.013$, $p = 0.0004$]. SIX3 enhanced *Per2* promoter-driven luciferase expression to a greater degree than VAX1 (Figure 6a,b, top, 8.8-fold vs. threefold induction). As ATTA sites are known consensus binding sequences for both SIX3 and VAX1, we sequentially mutated six ATTA-like sites within the regulatory region of *Per2* to determine which sites are involved in the observed modulatory effect (Table 1). Site-directed mutagenesis in intron 1 of *Per2*, at +1,319 bp, +1,770 bp, or +1,774 bp, preserved or significantly increased regulation by SIX3 (Figure 6a), but significantly reduced or abolished enhancement of expression by VAX1 (Figure 6b). Because the molecular clock is an oscillatory gene network, modulation of one of the clock genes can affect how the clock runs as a whole. To determine if modulation of *Per2* by SIX3 and VAX1 affects SCN clock function, we generated triple transgenic mice, crossing either *Six3^{syn}* or *Vax1^{syn}* mice with PER2::LUC knock-in reporter mice (*Six3^{syn}:PER2::LUC* and *Vax1^{syn}:PER2::LUC*). In diestrus/metestrus females, SCN slices from *Six3^{syn}* mice had a longer circadian period than controls (Figure 6c,e), whereas SCN slices from *Vax1^{syn}* mice had a period comparable to controls (Figure 6d,e). Interestingly, the two-way ANOVA mixed effect model revealed significant interactions between genotypes [$F_{(1,28)} = 31.91$, $p < 0.0001$], an overall effect of mouse strain [*Six3^{syn}:PER2::LUC* vs. *Vax1^{syn}:Per2::LUC*, $F_{(1,28)} = 15.18$, $p = 0.0006$], as well as an overall effect of genotype on the period of the clock [$F_{(1,28)} = 4.537$, $p = 0.0421$]. In contrast, no significant effect of *Six3* or *Vax1* conditional KO was observed on PER2::LUC amplitude (Figure 6f).

3.5 | Changes in time-of-day of peak PER2::LUC expression in the HPG axis are associated with abnormal ovarian function in *Six3^{syn}* female mice

Female fertility requires properly synchronized circadian rhythms among reproductive tissues to support ovulation. To determine if the impaired fertility of *Six3^{syn}* and *Vax1^{syn}* females was caused by mis-alignment of circadian rhythms in the reproductive axis, circadian phases (defined by time of PER2::LUC peak) were examined in SCN, pituitary, and ovary explants from diestrus/metestrus female *Six3^{fl/fl}:PER2::LUC* and *Six3^{syn}:PER2::LUC* mice (Figure 7a), as well as *Vax1^{fl/fl}:PER2::LUC* and *Vax1^{syn}: PER2::LUC* mice (Figure 7b). Compared to controls, SCN phase was significantly altered in both *Six3^{syn}:PER2::LUC* and *Vax1^{syn}:PER2::LUC* mice [Circular *t* test, *Six3^{syn}:PER2::LUC*: $F_{(1,17)} = 45.91$, $p < 0.001$; *Vax1^{syn}:PER2::LUC*: $F_{(1,19)} = 11.49$, $p = 0.003$], as was pituitary phase [*Six3^{syn}:PER2::LUC*: $F_{(1,9)} = 5.98$, $p = 0.04$; *Vax1^{syn}:PER2::LUC*: $F_{(1,21)} = 5.92$, $p = 0.02$]. In contrast, no significant change in ovary phase was detected in *Six3^{syn}* or *Vax1^{syn}* mice relative to controls [*Six3^{syn}:PER2::LUC*: $F_{(1,11)} = 3.71$, $p = 0.08$; *Vax1^{syn}:PER2::LUC*: $F_{(1,18)} = 4.13$, $p = 0.057$]. The change in phase of the SCN and pituitary could impact ovarian sensitivity to LH, or expression of the clock-controlled LH receptor (LHR) in ovarian follicles. To determine if ovarian function and sensitivity to LH might be changed, we super-ovulated *Six3^{fl/fl}* and *Six3^{syn}* females and counted the number of oocytes in the fallopian tubes. All *Six3^{fl/fl}* females super-ovulated as expected, but in contrast, three of five *Six3^{syn}* females did not respond to the treatment (Figure 7c). The reduced but not absent ovarian LH sensitivity of *Six3^{syn}* females is consistent with the subfertile reproductive phenotype. That is, *Six3^{syn}* females

infrequently generate litters (Figure 2a), but when they do generate a litter, the litter size is normal (Figure 7d), consistent with comparable corpora lutea numbers in $Six3^{fl/fl}$ and $Six3^{syn}$ females (Figure 2g).

Generating enough $Vax1^{syn}$ females for similar super-ovulation studies would have required a very large breeding colony, due to subfertility and high germline recombination frequency in this strain. Instead, to conserve animals, we performed LH receptor immunohistochemistry on ovaries collected from $Vax1^{syn}$ females at ZT2 and ZT12. Although our data were quite variable and sample size small, we observed a modest, non-significant increase in LH receptor expression in follicles at ZT12 versus ZT2, as expected (Mereness et al., 2016; Nakamura et al., 2010). However, only one to two follicles in each $Vax1^{syn}$ ovary had LH receptor expression, a number 5–10 times lower than in controls (Figure 7e,f). This suggests that $Vax1^{syn}$ ovaries might be less sensitive to LH at the time of the surge, which could contribute to the subfertility in these females (Figure 2b). Nevertheless, when $Vax1^{syn}$ females do have a litter, their litter size is comparable to controls (Figure 7d), suggesting that the HPG axis is functional when ovulation occurs.

4 | DISCUSSION

Here we identify novel roles for SIX3 and VAX1 in the brain. SIX3 and VAX1 regulate $Per2$ expression and circadian rhythmicity, and loss of SIX3 or VAX1 in neurons weakens circadian locomotor rhythms. Weakened SCN pacemaker output is associated with changes in circadian rhythm timing in the reproductive axis, loss of the LH surge, and reduced female fertility.

4.1 | Novel roles of SIX3 and VAX1 in the adult hypothalamus

$Six3$ and $Vax1$ are important for eye and brain development, whereas their roles in the post-developmental brain are far less studied. We confirmed that expression of both $Six3$ and $Vax1$ is maintained in the adult hypothalamus, and both genes are highly expressed in the SCN (Pandolfi, Breuer, et al., 2019; VanDunk et al., 2011). We recently showed that conditional deletion of $Vax1$ in the developing SCN impacts circadian rhythms of wheel-running activity (Pandolfi, Breuer, et al., 2019). To shed light on the post-developmental role of SIX3 and VAX1 in the SCN, we used the $Synapsin^{cre}$ allele, which targets most maturing and post-proliferating neurons in the brain. SCN size and morphology in $Six3^{syn}$ and $Vax1^{syn}$ mice were comparable to controls, indicating that $Synapsin^{cre}$ does not target the SCN before embryonic day 15, and can be used to evaluate gene function from late development onward.

One major limitation of the $Synapsin^{cre}$ allele is its broad targeting throughout the brain and peripheral reproductive organs. The targeting of the $Synapsin^{cre}$ allele to peripheral organs, however, is not expected to impact the observed phenotypes significantly, as $Six3$ and $Vax1$ are not expressed in the ovary or uterus. Both $Six3$ and $Vax1$ are expressed in the pituitary, but both conditional KO mouse lines had intact gonadotrope sensitivity to a GnRH challenge, and both mouse lines produced LH and FSH. Thus, a potential deletion of $Six3$ in a subset of gonadotropes is not likely to be the driving factor in the subfertility of $Six3^{syn}$ females. In the adult brain, $Synapsin^{cre}$ recombined the $Six3^{flox}$ and $Vax1^{flox}$ alleles

in all the studied brain areas, including the olfactory bulb, striatum, cortex, hippocampus, SCN, and paraventricular nucleus. *Six3* is broadly expressed in the late developing and adult brain, where it is important for striatal development; deletion of *Six3^flox/flox* in the striatum impairs medium spiny neuron plasticity and striatum function (Xu et al., 2018; Yang et al., 2021). As the striatum is important for motor function and reward behavior, we considered the possibility that *Six3* deletion in the striatum contributed to the impaired wheel-running behavior that we observed in *Six3^syn* females. However, the impaired wheel-running behavior was observed primarily in DD, and involves timing as well as amount of activity, which indicates that *Six3^syn* females have abnormal SCN output and is consistent with the known role of *Six3* in SCN function (VanDunk et al., 2011). In contrast to *Six3*, *Vax1* expression is limited to the olfactory bulb and ventral forebrain in late development and is primarily expressed in a subset of cells in the olfactory bulb, pituitary (but not in gonadotropes) (Hoffmann et al., 2014), testis, and SCN in adulthood. Thus, *Vax1^flox* allele recombination outside the hypothalamus is not expected to contribute significantly to the observed circadian and reproductive phenotypes observed in the *Vax1^syn* females.

Six3 and *Vax1* are both expressed in GnRH neurons, where deletion of *Vax1* causes a loss of GnRH expression, whereas deletion of *Six3* increases the number of GnRH-expressing neurons (Hoffmann et al., 2016; Pandolfi et al., 2018). We did not expect GnRH neuron numbers to be affected in *Vax1^syn* mice, as only <2% of GnRH neurons were targeted by *Synapsin^cre*. But surprisingly, we found a two-fold increase in the number of GnRH neurons in *Vax1^syn* mice. This suggests that *Vax1* expression in non-GnRH neurons might perhaps regulate the final number of GnRH-expressing neurons. One possible mechanism for increased survival or proliferation of developing GnRH neurons is prolonged or increased expression of Netrin-1, a guidance cue and survival factor regulated by VAX1 and required for GnRH neuron migration (Bertuzzi et al., 1999; Schwarting et al., 2004). The increase in GnRH-expressing neuron numbers in *Vax1^syn* mice did not significantly alter basal LH and FSH levels, nor the capacity of GnRH neurons to promote LH release in response to a kisspeptin challenge. This is consistent with other findings that increase in number of GnRH neurons has no significant impact on reproduction (Givens et al., 2005; Hoffmann et al., 2019; Pandolfi et al., 2018).

4.2 | Transcriptional regulation of *Per2* by SIX3 and VAX1 impacts SCN circadian output

One of the fundamental characteristics of SCN time-keeping function is its capacity to maintain ~24 hr rhythmicity within its neuronal network despite genetic perturbations that essentially abolish circadian rhythmicity in single SCN neurons (Liu et al., 2007). This robustness of the SCN circuit can conceal the role of genes in SCN network function and the contributions of neuronal subpopulations within the SCN to control behavior and neuroendocrine function.

To determine the roles of SIX3 and VAX1 in circadian timekeeping, we tested circadian locomotor activity rhythms of *Six3^syn* and *Vax1^syn* females. We found much weaker free-running circadian rhythms of locomotor activity in *Six3^syn* females, and more subtle impairment in *Vax1^syn* females. To study the SCN circadian clock more directly, we used the PER2::LUC reporter to examine rhythms in SCN explants, and found opposite effects on

circadian period in the two genotypes: longer period in *Six3^syn* SCN versus a non-significant trend for shorter period in *Vax1^syn* SCN. The lengthened period in the *Six3^syn:PER2::LUC* SCN reflected the longer free-running period that developed in behavioral rhythms of most *Six3^syn* mice after 3–4 weeks in DD (See bottom of Figure 3a, panels a3 and a4). These effects on SCN PER2::LUC period might be driven by modulation of *Per2* expression. Both SIX3 and VAX1 enhanced *Per2-luciferase* expression *in vitro*. Site-directed mutagenesis in intron 1 of *Per2* preserved or increased the enhanced expression by SIX3, but reduced or abolished the enhancement of expression by VAX1. This suggests that intron 1 contains regulatory elements that are differentially regulated by SIX3 and VAX1. However, as PER2::LUC amplitude was not significantly impacted in SCN explants, SIX3 and VAX1 may selectively regulate the period of the clock. It will be of interest in the future to determine if these opposite effects of SIX3 and VAX1 on period in SCN explants might arise from specific signaling complexes assembled by SIX3 and VAX1 on the ATTA-like sites identified in the *Per2* regulatory region. Interestingly, we observed differences in SIX3 and VAX1 effects at the SCN peptide promoters for *Avp* and *Vip*. SIX3 is a strong activator of *Avp*-driven expression in transient transfection assays, although immunohistochemistry for AVP in *Six3^syn* SCN did not reveal a significant reduction in AVP neuropeptide expression *in vivo*. VAX1, on the other hand, is a strong activator of the *Vip* promoter, and *Vax1^syn* mice did exhibit a significant reduction in both VIP and AVP expression in the SCN. It also remains possible that altered AVP or VIP release patterns could contribute to disrupted SCN output in these mice.

4.3 | Weakening of SCN output is associated with impaired LH surge at activity onset and female subfertility

A large amount of literature has shown that the timing and amplitude of the LH surge requires coincidence of a daily timing signal from the SCN with increased levels of estradiol to drive kisspeptin-promoted GnRH release at the median eminence (Christian et al., 2005; Christian & Moenter, 2008, 2010; Clarkson et al., 2008; Freeman, 1994; Goodman & Daniel, 1985; Herbison et al., 2008; Moenter et al., 1991; Piet et al., 2015). VIP and AVP projections to GnRH neurons and kisspeptin neurons, respectively, modulate the activity of these neurons (Christian & Moenter, 2008; Piet et al., 2015, 2016; Smith et al., 2000; Williams et al., 2011). Thus, changes in VIP and/or AVP neuron peptide expression or circadian rhythm function, as seen in *Six3^syn* and *Vax1^syn* mice, could be part of the mechanism underlying the lack of an LH surge around activity onset in these mice. Such a change in hypothalamic circuit function would explain why both of these conditional KO models have intact sensitivity to a kisspeptin challenge.

To explore how mistimed SCN rhythmic output may lead to loss of reproductive function in *Six3^syn* or *Vax1^syn* mice, we measured the time of peak PER2::LUC expression in the SCN, pituitary, and ovary using the well-validated circadian PER2::LUC reporter mouse (Yoo et al., 2004). In both *Six3^syn* and *Vax1^syn* mice, PER2::LUC phase was mistimed in the SCN and pituitary. Although the pituitary phase was advanced in both *Six3^syn* and *Vax1^syn* females, it is doubtful that this had a significant impact on fertility because (a) circadian rhythm disruption of pituitary gonadotropes only modestly impacts LH and FSH release (Chu et al., 2013), and (b) gonadotrope sensitivity to LH is maintained in both of our mouse

models. Of greater consequence, phases of the SCN shifted in opposite directions in *Six3^{syn}* and *Vax1^{syn}* females, without shifting the phase of the ovary, causing the SCN to be ~10–15 hr out of phase with the ovary in *Six3^{syn}* mice, and 5–6 hr out of phase in *Vax1^{syn}* mice. Such a large phase misalignment between the SCN and ovary would be expected to cause the LH surge at a time of day when there is low expression of LH receptors in ovarian theca cells, which is known to impair ovulation (Mereness et al., 2016). Indeed, superovulation was less efficient at promoting ovulation in *Six3^{syn}* females.

To test whether LH receptor expression in *Vax1^{syn}* mice showed the normal pattern of an increase at ZT12 (expected time of the LH surge), versus ZT2, we counted the number of ovarian follicles positive for LH receptor. Indeed, *Vax1^{syn}* females showed only a modest increase in LH receptor expression at ZT12, although the difference from control did not reach statistical significance. Overall, our data support the hypothesis that the absence of *Six3* or *Vax1* in the SCN weakens SCN output, leading to misaligned circadian rhythms in the reproductive axis, thereby reducing ovulation efficacy. The partial preservation of female fertility, with relatively rare but normally sized litters in both *Six3^{syn}* and *Vax1^{syn}* females, might be explained by some variability of this misalignment, such that the LH surge occasionally coincides with high ovarian LH receptor expression and allows for normal pregnancy.

Supplementary Material

Refer to Web version on PubMed Central for supplementary material.

ACKNOWLEDGMENTS

DATA AVAILABILITY STATEMENT

The data that support the findings of this study are available from the corresponding author upon reasonable request.

REFERENCES

Alvarez JD, Hansen A, Ord T, Bebas P, Chappell PE, Giebultowicz JM, Williams C, Moss S, & Sehgal A (2008). The circadian clock protein BMAL1 is necessary for fertility and proper testosterone production in mice. Journal of Biological Rhythms, 23(1), 26–36. 10.1177/0748730407311254 [PubMed: 18258755]

Bedont JL, & Blackshaw S (2015). Constructing the suprachiasmatic nucleus: A watchmaker's perspective on the central clockworks. Frontiers in Systems Neuroscience, 9, 74. 10.3389/fnsys.2015.00074 [PubMed: 26005407]

Bedont JL, LeGates TA, Slat EA, Byerly MS, Wang H, Hu J, Rupp AC, Qian J, Wong GW, Herzog ED, Hattar S, & Blackshaw S (2014). Lhx1 controls terminal differentiation and circadian function of the suprachiasmatic nucleus. Cell Reports, 7(3), 609–622. 10.1016/j.celrep.2014.03.060 [PubMed: 24767996]

Bertuzzi S, Hindges R, Mui SH, O'Leary DD, & Lemke G (1999).The homeodomain protein vax1 is required for axon guidance and major tract formation in the developing forebrain. Genes & Development, 13(23), 3092–3105. 10.1101/gad.13.23.3092 [PubMed: 10601035]

Bittman EL (2019). Circadian function in multiple cell types is necessary for proper timing of the preovulatory LH surge. Journal of Biological Rhythms, 34(6), 622–633. 10.1177/0748730419873511 [PubMed: 31530063]

Bronson FH, & Vom Saal FS (1979). Control of the preovulatory release of luteinizing hormone by steroids in the mouse. Endocrinology, 104(5), 1247–1255. 10.1210/endo-104-5-1247 [PubMed: 571329]

Cameo P, Szmidt M, Strakova Z, Mavrogianis P, Sharpe-Timms KL, & Fazleabas AT (2006). Decidualization regulates the expression of the endometrial chorionic gonadotropin receptor in the primate. Biology of Reproduction, 75(5), 681–689. 10.1095/biolreprod.106.051805 [PubMed: 16837644]

Challet E (2015). Keeping circadian time with hormones. Diabetes, Obesity & Metabolism, 17(Suppl 1), 76–83. 10.1111/dom.12516

Choe HK, Kim H-D, Park SH, Lee H-W, Park J-Y, Seong JY, Lightman SL, Son GH, & Kim K (2013). Synchronous activation of gonadotropin-releasing hormone gene transcription and secretion by pulsatile kisspeptin stimulation. Proceedings of the National Academy of Sciences of the United States of America, 110(14), 5677–5682. 10.1073/pnas.1213594110 [PubMed: 23509283]

Christian CA, Mobley JL, & Moenter SM (2005). Diurnal and estradiol-dependent changes in gonadotropin-releasing hormone neuron firing activity. Proceedings of the National Academy of Sciences of the United States of America, 102(43), 15682–15687. 10.1073/pnas.0504270102 [PubMed: 16230634]

Christian CA, & Moenter SM (2008). Vasoactive intestinal polypeptide can excite gonadotropin-releasing hormone neurons in a manner dependent on estradiol and gated by time of day. Endocrinology, 149(6), 3130–3136. 10.1210/en.2007-1098 [PubMed: 18326000]

Christian CA, & Moenter SM (2010). The neurobiology of preovulatory and estradiol-induced gonadotropin-releasing hormone surges. Endocrine Reviews, 31(4), 544–577. 10.1210/er.2009-0023 [PubMed: 20237240]

Chu A, Zhu L, Blum ID, Mai O, Leliavski A, Fahrenkrug J, Oster H, Boehm U, & Storch K-F (2013). Global but not gonadotrope-specific disruption of Bmal1 abolishes the luteinizing hormone surge without affecting ovulation. Endocrinology, 154(8), 2924–2935. 10.1210/en.2013-1080 [PubMed: 23736292]

Clark DD, Gorman MR, Hatori M, Meadows JD, Panda S, & Mellon PL (2013). Aberrant development of the suprachiasmatic nucleus and circadian rhythms in mice lacking the homeodomain protein

six6. Journal of Biological Rhythms, 28(1), 15–25. 10.1177/0748730412468084 [PubMed: 23382588]

Clarkson J, d'Anglemont de Tassigny X, Moreno AS, Colledge WH, & Herbison AE (2008). Kisspeptin-GPR54 signaling is essential for preovulatory gonadotropin-releasing hormone neuron activation and the luteinizing hormone surge. Journal of Neuroscience, 28(35), 8691–8697. 10.1523/JNEUROSCI.1775-08.2008 [PubMed: 18753370]

Freeman ME (1994). The neuroendocrine control of the ovarian cycle of the rat. In Knobil E, Neill JD, Greenwald GS, Market CL, & Pfaff DW (Eds.), The physiology of reproduction (2nd ed., pp. 613–658). Raven Press.

Givens ML, Rave-Harel N, Goonewardena VD, Kurotani R, Berdy SE, Swan CH, Rubenstein JLR, Robert B, & Mellon PL (2005). Developmental regulation of gonadotropin-releasing hormone gene expression by the MSX and DLX homeodomain protein families. Journal of Biological Chemistry, 280(19), 19156–19165. 10.1074/jbc.M502004200

Goodman RL, & Daniel K (1985). Modulation of pulsatile luteinizing hormone secretion by ovarian steroids in the rat. Biology of Reproduction, 32(2), 217–225. [PubMed: 3986263]

Hatori M, Gill S, Mure LS, Goulding M, O'Leary DD, & Panda S (2014). Lhx1 maintains synchrony among circadian oscillator neurons of the SCN. eLife, 3, e03357. 10.7554/eLife.03357 [PubMed: 25035422]

Herbison AE, Porteous R, Pape JR, Mora JM, & Hurst PR (2008). Gonadotropin-releasing hormone (GnRH) neuron requirements for puberty, ovulation and fertility. Endocrinology, 149(2), 597–604. [PubMed: 18006629]

Hoffmann HM (2018). Determination of reproductive competence by confirming pubertal onset and performing a fertility assay in mice and rats. Journal of Visualized Experiments, 140, e58352. 10.3791/58352

Hoffmann HM, Gong P, Tamrazian A, & Mellon PL (2018). Transcriptional interaction between cFOS and the homeodomain-binding transcription factor VAX1 on the GnRH promoter controls Gnrh1 expression levels in a GnRH neuron maturation specific manner. Molecular and Cellular Endocrinology, 461, 143–154. 10.1016/j.mce.2017.09.004 [PubMed: 28890143]

Hoffmann HM, Larder R, Lee JS, Hu RJ, Trang C, Devries BM, Clark DD, & Mellon PL (2019). Differential CRE expression in Lhrh-Cre and Gnrh-Cre alleles and the impact on fertility in Otx2-flox mice. Neuroendocrinology, 108(4), 328–342. 10.1159/000497791 [PubMed: 30739114]

Hoffmann HM, Pandolfi EC, Larder R, & Mellon PL (2019). Haploinsufficiency of homeodomain proteins Six3, Vax1, and Otx2, causes subfertility in mice via distinct mechanisms. Neuroendocrinology, 109(3), 200–207. 10.1159/000494086 [PubMed: 30261489]

Hoffmann HM, Tamrazian A, Xie H, Perez-Millan MI, Kauffman AS, & Mellon PL (2014). Heterozygous deletion of ventral anterior homeobox (vax1) causes subfertility in mice. Endocrinology, 155(10), 4043–4053. 10.1210/en.2014-1277 [PubMed: 25060364]

Hoffmann HM, Trang C, Gong P, Kimura I, Pandolfi EC, & Mellon PL (2016). Deletion of Vax1 from GnRH neurons abolishes GnRH expression and leads to hypogonadism and infertility. Journal of Neuroscience, 36(12), 3506–3518. 10.1523/JNEUROSCI.2723-15.2016 [PubMed: 27013679]

Horvath TL, Cela V, & van der Beek EM (1998). Gender-specific apposition between vasoactive intestinal peptide-containing axons and gonadotrophin-releasing hormone-producing neurons in the rat. Brain Research, 795(1–2), 277–281. 10.1016/S0006-8993(98)00208-X [PubMed: 9622650]

Kumar P, & Sait SF (2011). Luteinizing hormone and its dilemma in ovulation induction. Journal of Human Reproductive Sciences, 4(1), 2–7. 10.4103/0974-1208.82351 [PubMed: 21772731]

Kumar TR, Low MJ, & Matzuk MM (1998). Genetic rescue of follicle-stimulating hormone beta-deficient mice. Endocrinology, 139(7), 3289–3295. [PubMed: 9645705]

Kumar TR, Wang Y, Lu N, & Matzuk MM (1997). Follicle stimulating hormone is required for ovarian follicle maturation but not male fertility. Nature Genetics, 15(2), 201–204. 10.1038/ng0297-201 [PubMed: 9020850]

Larder R, Clark DD, Miller NL, & Mellon PL (2011). Hypothalamic dysregulation and infertility in mice lacking the homeodomain protein Six6. Journal of Neuroscience, 31(2), 426–438. 10.1523/JNEUROSCI.1688-10.2011 [PubMed: 21228153]

Lehman MN, Silver R, Gladstone WR, Kahn RM, Gibson M, & Bittman EL (1987). Circadian rhythmicity restored by neural transplant. Immunocytochemical characterization of the graft and its integration with the host brain. Journal of Neuroscience, 7(6), 1626–1638. [PubMed: 3598638]

Liu AC, Welsh DK, Ko CH, Tran HG, Zhang EE, Priest AA, Buhr ED, Singer O, Meeker K, Verma IM, Doyle FJ,Takahashi JS, & Kay SA (2007). Intercellular coupling confers robustness against mutations in the SCN circadian clock network. Cell, 129(3), 605–616. 10.1016/j.cell.2007.02.047 [PubMed: 17482552]

Liu W, Lagutin OV, Mende M, Streit A, & Oliver G (2006). Six3 activation of Pax6 expression is essential for mammalian lens induction and specification. EMBO Journal, 25(22), 5383–5395. 10.1038/sj.emboj.7601398

Livak KJ, & Schmittgen TD (2001). Analysis of relative gene expression data using real-time quantitative PCR and the 2(-Delta Delta C(T)) Method. Methods, 25(4), 402–408. 10.1006/meth.2001.1262 [PubMed: 11846609]

Loh DH, Kuljis DA, Azuma L, Wu Y, Truong D, Wang HB, & Colwell CS (2014). Disrupted reproduction, estrous cycle, and circadian rhythms in female mice deficient in vasoactive intestinal peptide. Journal of Biological Rhythms, 29(5), 355–369. 10.1177/0748730414549767 [PubMed: 25252712]

Ma X, Dong Y, Matzuk MM, & Kumar TR (2004). Targeted disruption of luteinizing hormone beta-subunit leads to hypogonadism, defects in gonadal steroidogenesis, and infertility. Proceedings of the National Academy of Sciences of the United States of America, 101(49), 17294–17299. [PubMed: 15569941]

Mahoney MM (2010). Shift work, jet lag, and female reproduction. International Journal of Endocrinology, 2010, 813764. 10.1155/2010/813764 [PubMed: 20224815]

Meczekalski B, Katulski K, Czyzyk A, Podfigurna-Stopa A, & Maciejewska-Jeske M (2014). Functional hypothalamic amenorrhea and its influence on women's health. Journal of Endocrinological Investigation, 37(11), 1049–1056. 10.1007/s40618-014-0169-3 [PubMed: 25201001]

Mereness AL, Murphy ZC, Forrestel AC, Butler S, Ko C, Richards JS, & Sellix MT (2016). Conditional deletion of Bmal1 in ovarian theca cells disrupts ovulation in female mice. Endocrinology, 157(2), 913–927. 10.1210/en.2015-1645 [PubMed: 26671182]

Meyer-Bernstein EL, Jetton AE, Matsumoto SI, Markuns JF, Lehman MN, & Bittman EL (1999). Effects of suprachiasmatic transplants on circadian rhythms of neuroendocrine function in golden hamsters. Endocrinology, 140(1), 207–218. 10.1210/endo.140.1.6428 [PubMed: 9886827]

Miller BH, Olson SL, Levine JE, Turek FW, Horton TH, & Takahashi JS (2006). Vasopressin regulation of the proestrous luteinizing hormone surge in wild-type and Clock mutant mice. Biology of Reproduction, 75(5), 778–784. 10.1095/biolreprod.106.052845 [PubMed: 16870944]

Moenter SM, Caraty A, Locatelli A, & Karsch FJ (1991). Pattern of gonadotropin-releasing hormone (GnRH) secretion leading up to ovulation in the ewe: Existence of a preovulatory GnRH surge. Endocrinology, 129(3), 1175–1182. [PubMed: 1874164]

Moller-Levet CS, Archer SN, Bucca G, Laing EE, Slak A, Kabiljo R, Lo JCY, Santhi N, von Schantz M, Smith CP, & Dijk D-J (2013). Effects of insufficient sleep on circadian rhythmicity and expression amplitude of the human blood transcriptome. Proceedings of the National Academy of Sciences of the United States of America, 110(12), E1132–E1141. 10.1073/pnas.1217154110 [PubMed: 23440187]

Moore RY, & Eichler VB (1972). Loss of a circadian adrenal corticosterone rhythm following suprachiasmatic lesions in rat. Brain Research, 42, 201–206. [PubMed: 5047187]

Mori H, Hanada R, Hanada T, Aki D, Mashima R, Nishinakamura H, Torisu T, Chien KR, Yasukawa H, & Yoshimura A (2004). Socs3 deficiency in the brain elevates leptin sensitivity and confers resistance to diet-induced obesity. Nature Medicine, 10(7), 739–743. 10.1038/nm1071

Nakamura TJ, Sellix MT, Kudo T, Nakao N, Yoshimura T, Ebihara S, Colwell CS, & Block GD (2010). Influence of the estrous cycle on clock gene expression in reproductive tissues: Effects of fluctuating ovarian steroid hormone levels. Steroids, 75(3), 203–212. 10.1016/j.steroids.2010.01.007 [PubMed: 20096720]

Palm IF, Van Der Beek EM, Wiegant VM, Buijs RM, & Kalsbeek A (1999). Vasopressin induces a luteinizing hormone surge in ovariectomized, estradiol-treated rats with lesions of the suprachiasmatic nucleus. Neuroscience, 93(2), 659–666. 10.1016/S0306-4522(99)00106-2 [PubMed: 10465449]

Pandolfi EC, Breuer JA, Huu VA, Talluri T, Nguyen D, Lee JS, Hu R, Bharti K, Skowronska-Krawczyk D, Gorman MR, & Mellon PL (2019). The homeodomain transcription factors Vax1 and Six6 are required for SCN development and function. Molecular Neurobioiogy, 57(2), 1217–1232.

Pandolfi EC, Hoffmann HM, Schoeller EL, Gorman MR, & Mellon PL (2018). Haploinsufficiency of SIX3 abolishes male reproductive behavior through disrupted olfactory development, and impairs female fertility through disrupted GnRH neuron migration. Molecular Neurobioiogy, 55(11), 8709–8727. 10.1007/s12035-018-1013-0

Pandolfi EC, Tonsfeldt KJ, Hoffmann HM, & Mellon PL (2019). Deletion of the homeodomain protein Six6 from GnRH neurons decreases GnRH gene expression resulting in infertility. Endocrinology, 160(9), 2151–2164. 10.1210/en.2019-00113 [PubMed: 31211355]

Piet R, Dunckley H, Lee K, & Herbison AE (2016). Vasoactive intestinal peptide excites GnRH neurons in male and female mice. Endocrinology, 157(9), 3621–3630. 10.1210/en.2016-1399 [PubMed: 27501185]

Piet R, Fraissenon A, Boehm U, & Herbison AE (2015). Estrogen permits vasopressin signaling in preoptic kisspeptin neurons in the female mouse. Journal of Neuroscience, 35(17), 6881–6892. 10.1523/JNEUROSCI.4587-14.2015 [PubMed: 25926463]

Preibisch S, Saalfeld S, & Tomancak P (2009). Globally optimal stitching of tiled 3D microscopic image acquisitions. Bioinformatics, 25(11), 1463–1465. 10.1093/bioinformatics/btp184 [PubMed: 19346324]

Ralph MR, Foster RG, Davis FC, & Menaker M (1990). Transplanted suprachiasmatic nucleus determines circadian period. Science, 247, 975–978. 10.1126/science.2305266 [PubMed: 2305266]

Rempe D, Vangeison G, Hamilton J, Li Y, Jepson M, & Federoff HJ (2006). Synapsin I Cre transgene expression in male mice produces germline recombination in progeny. Genesis, 44(1):44–9. PMID: 16419044. 10.1002/gene.20183 [PubMed: 16419044]

Reppert SM, & Weaver DR (2002). Coordination of circadian timing in mammals. Nature, 418(6901), 935–941. [PubMed: 12198538]

Russo KA, La JL, Stephens SBZ, Poling MC, Padgaonkar NA, Jennings KJ, Piekarski DJ, Kauffman AS, & Kriegsfeld LJ (2015). Circadian control of the female reproductive axis through gated responsiveness of the RFRP-3 system to VIP signaling. Endocrinology, 156(7), 2608–2618. 10.1210/en.2014-1762 [PubMed: 25872006]

Salvador LM, Mukherjee S, Kahn RA, Lamm MLG, Fazleabas AT, Maizels ET, Bader M-F, Hamm H, Rasenick MM, Casanova JE, & Hunzicker-Dunn M (2001). Activation of the luteinizing hormone/choriogonadotropin hormone receptor promotes ADP ribosylation factor 6 activation in porcine ovarian follicular membranes. Journal of Biological Chemistry, 276(36), 33773–33781. 10.1074/jbc.M101498200

Schafer D, Kane G, Colledge WH, Piet R, & Herbison AE (2018). Sex- and sub region-dependent modulation of arcuate kisspeptin neurones by vasopressin and vasoactive intestinal peptide. Journal of Neuroendocrinology, 30(12), e12660. 10.1111/jne.12660 [PubMed: 30422333]

Schwarting GA, Raitcheva D, Bless EP, Ackerman SL, & Tobet S (2004). Netrin 1-mediated chemoattraction regulates the migratory pathway of LHRH neurons. European Journal of Neuroscience, 19(1), 11–20. 10.1111/j.1460-9568.2004.03094.x

Sen A, & Hoffmann HM (2019). Role of core circadian clock genes in hormone release and target tissue sensitivity in the reproductive axis. Molecular and Cellular Endocrinology, 501, 110655. 10.1016/j.mce.2019.110655 [PubMed: 31756424]

Shapiro RA, Xu C, & Dorsa DM (2000). Differential transcriptional regulation of rat vasopressin gene expression by estrogen receptor alpha and beta. Endocrinology, 141(11), 4056–4064. 10.1210/endo.141.11.7796 [PubMed: 11089536]

Shinozaki A, Misawa K, Ikeda Y, Haraguchi A, Kamagata M, Tahara Y, & Shibata S (2017). Potent effects of flavonoid nobiletin on amplitude, period, and phase of the circadian clock rhythm in PER2:LUCIFERASE mouse embryonic fibroblasts. PLoS ONE, 12(2), e0170904. 10.1371/journal.pone.0170904 [PubMed: 28152057]

Smarr BL, Gile JJ, & de la Iglesia HO (2013). Oestrogen-independent circadian clock gene expression in the anteroventral periventricular nucleus in female rats: Possible role as an integrator for circadian and ovarian signals timing the luteinising hormone surge. Journal of Neuroendocrinology, 25(12), 1273–1279. 10.1111/jne.12104 [PubMed: 24028332]

Smith MJ, Jiennes L, & Wise PM (2000). Localization of the VIP2 receptor protein on GnRH neurons in the female rat. Endocrinology, 141(11), 4317–4320. 10.1210/endo.141.11.7876 [PubMed: 11089568]

Sokolove PG, & Bushell WN (1978). The chi square periodogram: Its utility for analysis of circadian rhythms. Journal of Theoretical Biology, 72(1), 131–160. 10.1016/0022-5193(78)90022-x [PubMed: 566361]

Stephan FK, & Zucker I (1972). Circadian rhythms in drinking behavior and locomotor activity of rats are eliminated by hypothalamic lesions. Proceedings of the National Academy of Sciences of the United States of America, 69, 1583–1586. 10.1073/pnas.69.6.1583 [PubMed: 4556464]

van der Beek EM, Horvath TL, Wiegant VM, van den Hurk R, & Buijs RM (1997). Evidence for a direct neuronal pathway from the suprachiasmatic nucleus to the gonadotropin-releasing hormone system: Combined tracing and light and electron microscopic immunocytochemical studies. Journal of Comparative Neurology, 384(4), 569–579. 10.1002/(SICI)1096-9861(19970811)384:4<569:AID-CNE6>3.0.CO;2-0

VanDunk C, Hunter LA, & Gray PA (2011). Development, maturation, and necessity of transcription factors in the mouse suprachiasmatic nucleus. Journal of Neuroscience, 31(17), 6457–6467. 10.1523/JNEUROSCI.5385-10.2011 [PubMed: 21525287]

Vida B, Deli L, Hrabovszky E, Kalamatianos T, Caraty A, Coen CW, Liposits Z, & Kalló I (2010). Evidence for suprachiasmatic vasopressin neurones innervating kisspeptin neurones in the rostral periventricular area of the mouse brain: Regulation by oestrogen. Journal of Neuroendocrinology, 22(9), 1032–1039. 10.1111/j.1365-2826.2010.02045.x [PubMed: 20584108]

Welsh DK, Takahashi JS, & Kay SA (2010). Suprachiasmatic nucleus: Cell autonomy and network properties. Annual Review of Physiology, 72, 551–577. 10.1146/annurev-physiol-021909-135919

Welsh DK, Yoo SH, Liu AC, Takahashi JS, & Kay SA (2004). Bioluminescence imaging of individual fibroblasts reveals persistent, independently phased circadian rhythms of clock gene expression. Current Biology, 14(24), 2289–2295. 10.1016/j.cub.2004.11.057 [PubMed: 15620658]

Williams WP 3rd, Jarjisian SG, Mikkelsen JD, & Kriegsfeld LJ (2011). Circadian control of kisspeptin and a gated GnRH response mediate the preovulatory luteinizing hormone surge. Endocrinology, 152(2), 595–606. 10.1210/en.2010-0943 [PubMed: 21190958]

Williams WP 3rd, & Kriegsfeld LJ (2012). Circadian control of neuroendocrine circuits regulating female reproductive function. Frontiers in Endocrinology, 3, 60. 10.3389/fendo.2012.00060 [PubMed: 22661968]

Xu Z, Liang Q, Song X, Zhang Z, Lindtner S, Li Z, & Yang Z (2018). SP8 and SP9 coordinately promote D2-type medium spiny neuron production by activating Six3 expression. Development, 145(14), 165456. 10.1242/dev.165456

Yang L, Su Z, Wang Z, Li Z, Shang Z, Du H, Liu G, Qi D, Yang Z, Xu Z, & Zhang Z (2021). Transcriptional profiling reveals the transcription factor networks regulating the survival of striatal neurons. bioRxiv, 2020.2005.2020.105585.

Yoo S-H, Yamazaki S, Lowrey PL, Shimomura K, Ko CH, Buhr ED, Siepka SM, Hong H-K, Oh WJ, Yoo OJ, Menaker M, & Takahashi JS (2004). PERIOD2:LUCIFERASE real-time reporting of circadian dynamics reveals persistent circadian oscillations in mouse peripheral tissues. Proceedings of the National Academy of Sciences of the United States of America, 101(15), 5339–5346. 10.1073/pnas.0308709101 [PubMed: 14963227]

Zhu Y, Romero MI, Ghosh P, Ye Z, Charnay P, Rushing EJ, & Parada LF (2001). Ablation of NF1 function in neurons induces abnormal development of cerebral cortex and reactive gliosis in the brain. Genes & Development, 15(7), 859–876. 10.1101/gad.862101 [PubMed: 11297510]

Significance

Disruption of circadian rhythms, by light at night or genetic mutation, leads to increased risk of metabolic disorders and impaired cognitive and reproductive function. The brain's primary circadian pacemaker, the suprachiasmatic nucleus (SCN), translates light information into physiological signals. Here, we identify the transcription factors *Vax1* and *Six3* as required to generate a coherent circadian output signal from the SCN. Deletion of *Vax1* or *Six3* in neurons, including the SCN, dysregulates circadian rhythms in the reproductive axis, and is associated with female subfertility and mistimed hormone release. These studies advance our understanding of genes important for SCN circadian rhythm generation and fertility.
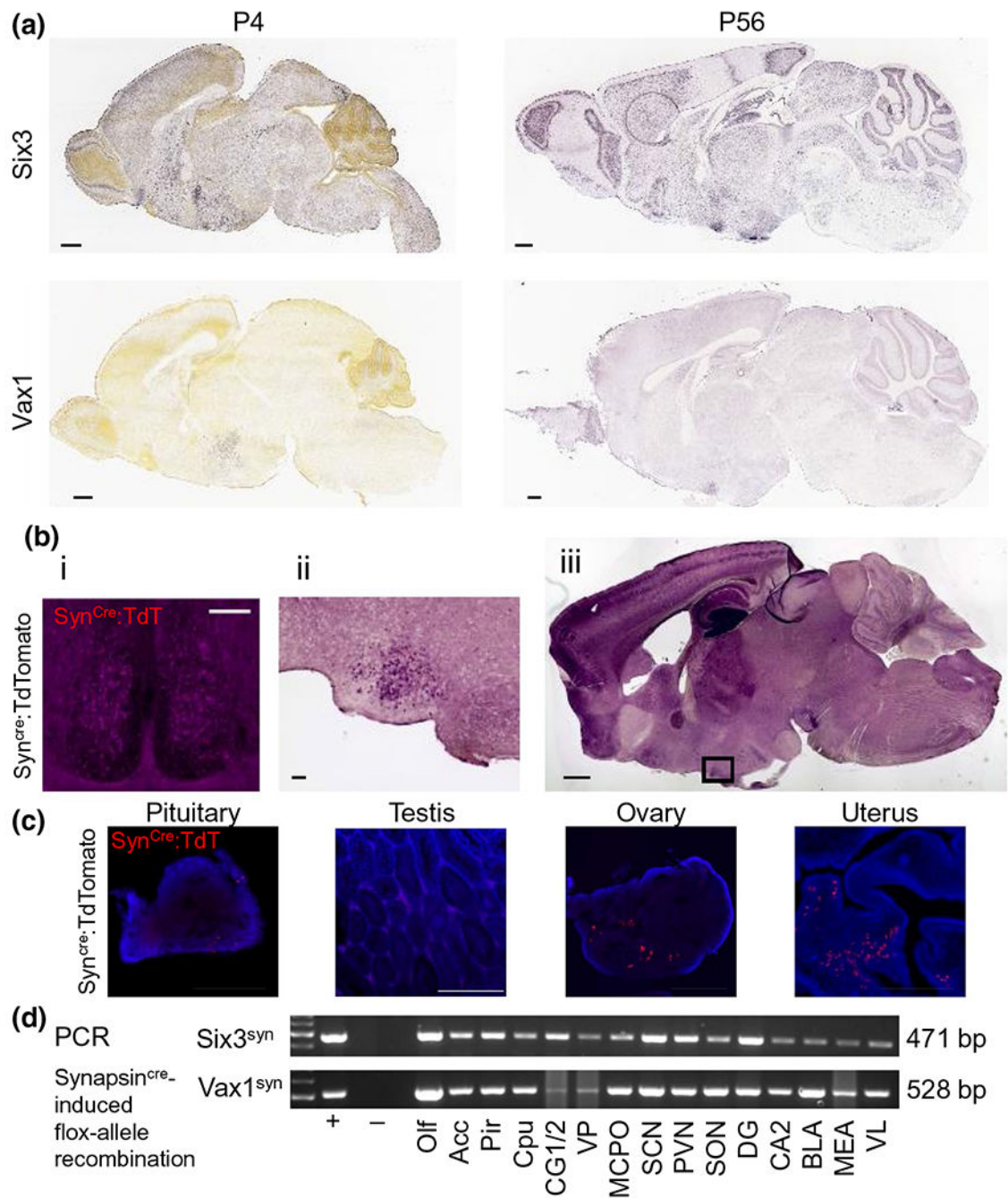
FIGURE 1.

SIX3 and VAX1 expression patterns and overlap with *Synapsin^cre*. (a) Allen Brain Atlas sagittal *in situ* hybridization images of *Six3* and *Vax1* expression patterns in the brain at postnatal day 4 (P4) and P56 in male. Scale bars 500 μm. (b) *Synapsin^cre* efficiently recombines the *Rosa26 tdTomato* allele in the SCN in *Synapsin^cre:tdTomato* mice. (i) *tdTomato* (magenta) presence in the adult female SCN. Scale bar 100 μm. (ii) Sagittal section containing the SCN, stained for tdTomato (RFP). Scale bar 100 μm. (iii) sagittal image of tdTomato (RFP) in an adult male (scale bar 500 μm). Dashed lines indicate

zoomed area in (ii). (c) *Synapsin^cre* recombines the *Rosa26 tdTomato* allele in the pituitary (female), ovary, and uterus, and not in the testis. Scale bar 500 μm. (d) PCR to assay *Synapsin^cre* driven recombination of the *Six3^flox* and *Vax1^flox* alleles in the female brain. Acc, nucleus accumbens; BLA, basolateral amygdala; CA2, hippocampal area CA2; CG1/2, cingulate cortex; Cpu, caudate putamen (striatum); DG, dentate gyrus; MCPO, magnocellular preoptic nucleus; MEA, medial amygdala; Olf, olfactory bulb; Pir, piriform cortex; PVN, paraventricular nucleus; SCN, suprachiasmatic nucleus; SON, supraoptic nucleus; VL, ventrolateral thalamic nucleus; VP, ventral pallidum. Representative images of $n = 3$
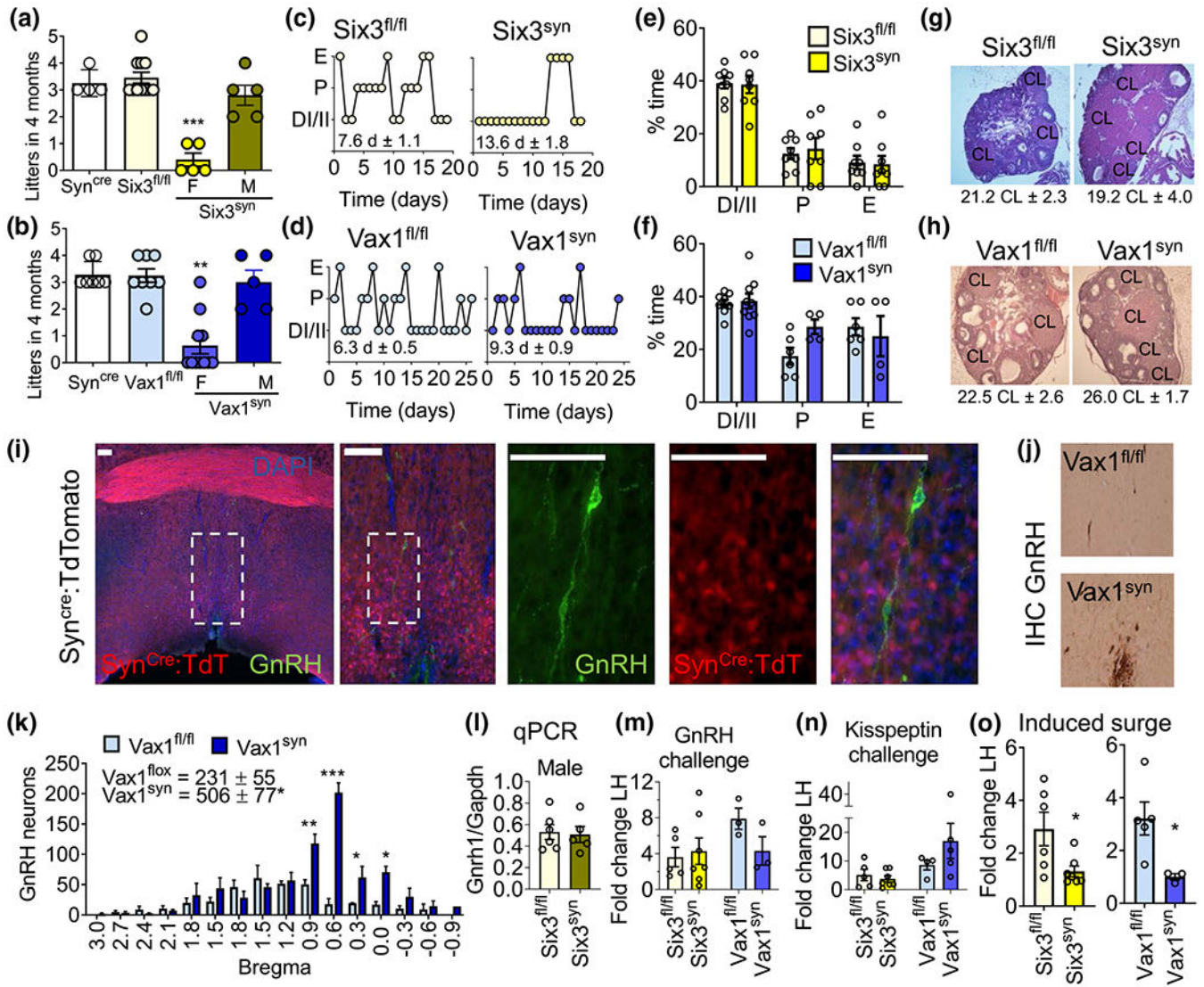
FIGURE 2.
Disrupted LH surge in *Six3^syn* and *Vax1^syn* female mice causing female subfertility. (a,b) A 4-month fertility study evaluating the number of litters born. (a) *Synapsin^cre* male x B6 female (*Syn^cre*), *Six3^fl/fl* x *Six3^fl/fl* (*Six3^fl/fl*) matings and *Six3^syn* x *Six3^fl/fl* or (b) B6 female x *Synapsin^cre* male (*Syn^cre*), *Vax1^fl/fl* x *Vax1^fl/fl* (*Vax1^fl/fl*) and *Vax1^syn* x *Vax1^fl/fl* matings. Statistical analysis by one-way ANOVA, compared to control (*Syn^cre*); ** $p < 0.01$; *** $p < 0.001$, $n = 5–11$. (c,d) Estrus cycling was monitored daily in adult females. DI/II, diestrus I/II; E, estrus; P, proestrus; (e,f) % time spent in each cycle. Statistical analysis by two-way ANOVA, $n = 6–8$. (g,h) Representative H&E images of ovarian morphology. CL, corpora lutea counted throughout the ovary, t test, $p > 0.05$, $n = 4–5$. Magnification ×4. (i) *Synapsin^cre* efficiently recombines the *Rosa26 tdTomato* (magenta) allele in female neurons, but does not appreciably target GnRH neurons (green) in the preoptic area, scale bar 100 μm. Representative images of $n = 4$. (j) Illustrative images of GnRH immunohistochemistry in the preoptic area of a female mouse in adulthood. Magnification ×20. (k) Quantification of number of GnRH neurons in male and female *Vax1^fl/fl* and *Vax1^syn* mice as determined

by immunohistochemistry for GnRH, $n = 3$–5, Student's t test (for total numbers of GnRH neurons) and two-way ANOVA for comparisons across Bregma *$p < 0.05$; **$p < 0.01$; ***$p < 0.001$. (I) qRT-PCR of whole hypothalamus for *Gnrh1* and *Gapdh* in *Six3^{fl/fl}* and *Six3^{syn}* males. Student's t test, $p > 0.05$, $n = 5$–6. (m) LH release in response to a bolus GnRH challenge (10 min) in diestrus/metestrus females. Student's t test, $p > 0.05$. $n = 4$–8. (n) LH release in response to a bolus kisspeptin challenge (*Six3^{syn}* 10 min, *Vax1^{syn}* 15 min) in diestrus/metestrus females. Student's t test, *$p < 0.05$, $n = 4$–7. (o) LH levels were evaluated in ovariectomized, estrogen primed females at ZT4 and ZT12.30, and fold change of ZT12.30/ZT4 in LH levels determined. Student's t test, *$p < 0.05$, $n = 3$–7
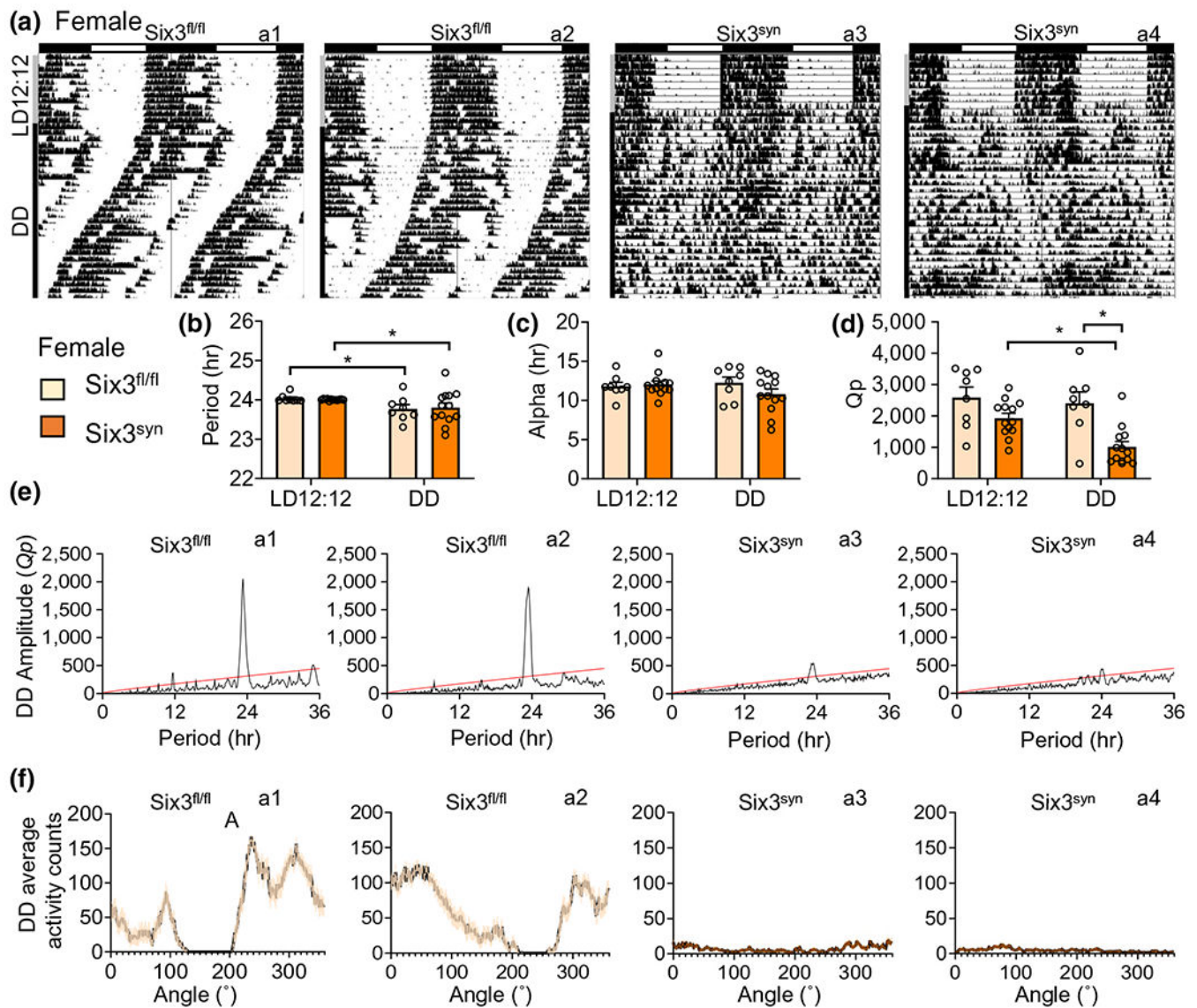
FIGURE 3.

Disrupted free-running locomotor activity rhythms in *Six3^syn* females. (a) Running-wheel activity patterns in *Six3^fl/fl* (*n* = 8) and *Six3^syn* (*n* = 13) female mice. Data show double plotted actogram activity with 10 days in LD12:12 (LD) followed by 28 days in constant darkness (DD). Data are presented in ClockLab normalized format. Horizontal bar above the actograms indicates lights on (white) and lights off (black) during the LD12:12 cycle. (b–d) Female 14-day average data for indicated analysis parameter in LD12:12 and DD. (e) χ^2 periodograms for females during 2 weeks in DD. Significance line (set at 0.001) is depicted in red. (f) Running-wheel activity profiles adjusted for estimated free running period in *Six3^fl/fl* and *Six3^syn* female mice in DD. *SEM* is indicated by orange shading. Estimated tau calculated via χ^2 were as follows; a1 tau = 23.3, a2 tau = 23.5, a3 tau = 24, a4 tau = 24.2. Statistical analysis by two-way repeated measures ANOVA mixed effect analysis, *n* = 7–13. Matching codes (a1, a2, etc.) on the upper right corner of each actogram, χ^2 periodogram, and activity profile indicate data from a particular mouse
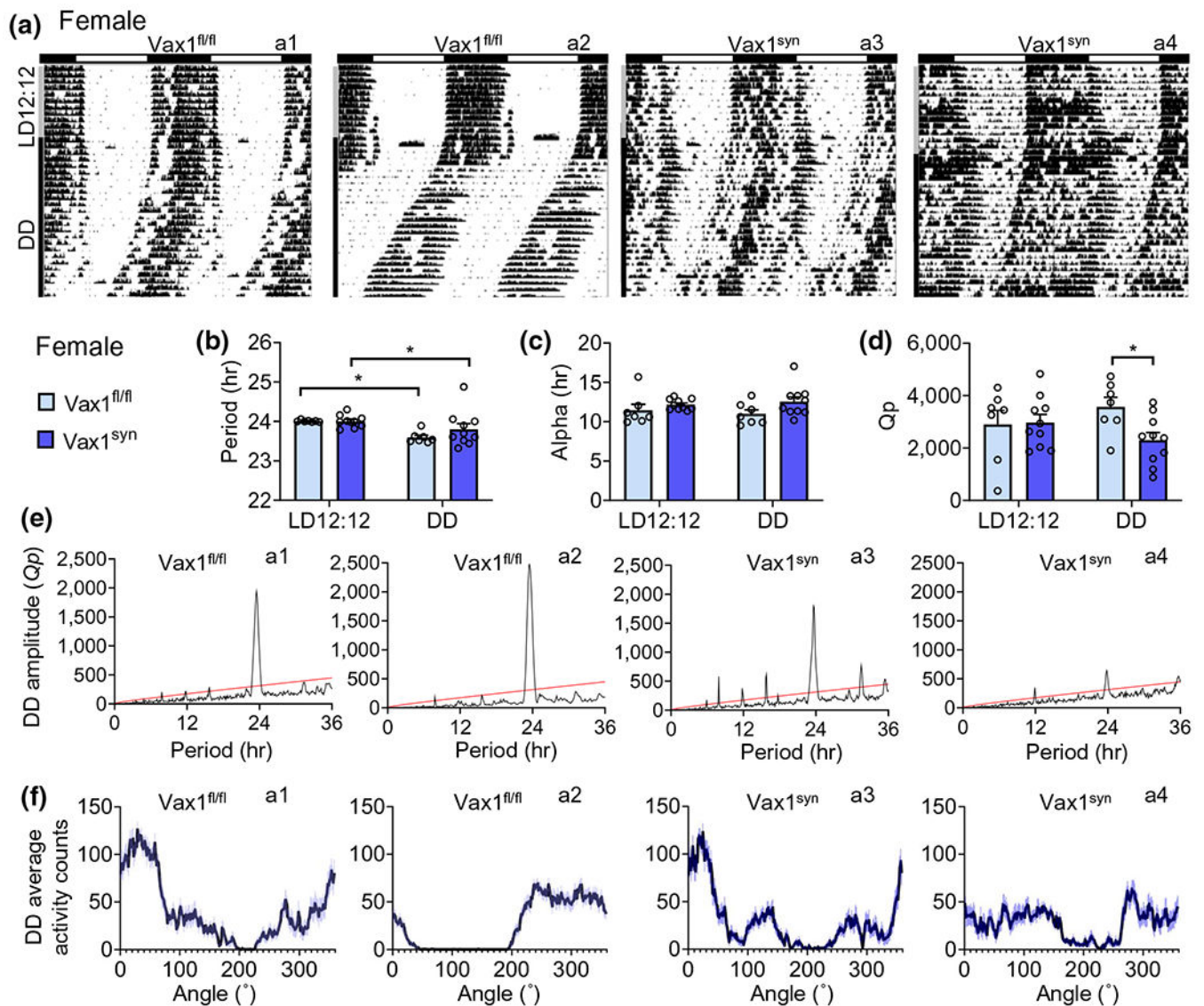
FIGURE 4.

Disrupted wheel-running activity in DD of *Vax1syn* females. (a) Running-wheel activity patterns in *Vax1fl/fl* ($n = 7$) and *Vax1syn* ($n = 10$) female mice. Format and indications as in Figure 3. (b–d) Female 14-day average data for indicated analysis parameter in LD12:12 and DD. (e) χ^2 periodograms for females during 2 weeks in DD. Significance line (set at 0.001) is depicted in red. (f) Running-wheel activity profiles adjusted for estimated free running period in *Vax1fl/fl* and *Vax1syn* female mice in DD. *SEM* is indicated by blue shading. Estimated tau, calculated via χ^2 were as follows; a1 tau = 23.5, a2 tau = 23.5, a3 tau = 23.6, a4 tau = 23.8. Statistical analysis by two-way repeated measures ANOVA mixed effect analysis, $n = 7$–13. Matching codes (a1, a2, etc.) on the upper right corner of each actogram, χ^2 periodogram and activity profile indicate data from a particular mouse, $p < 0.05$
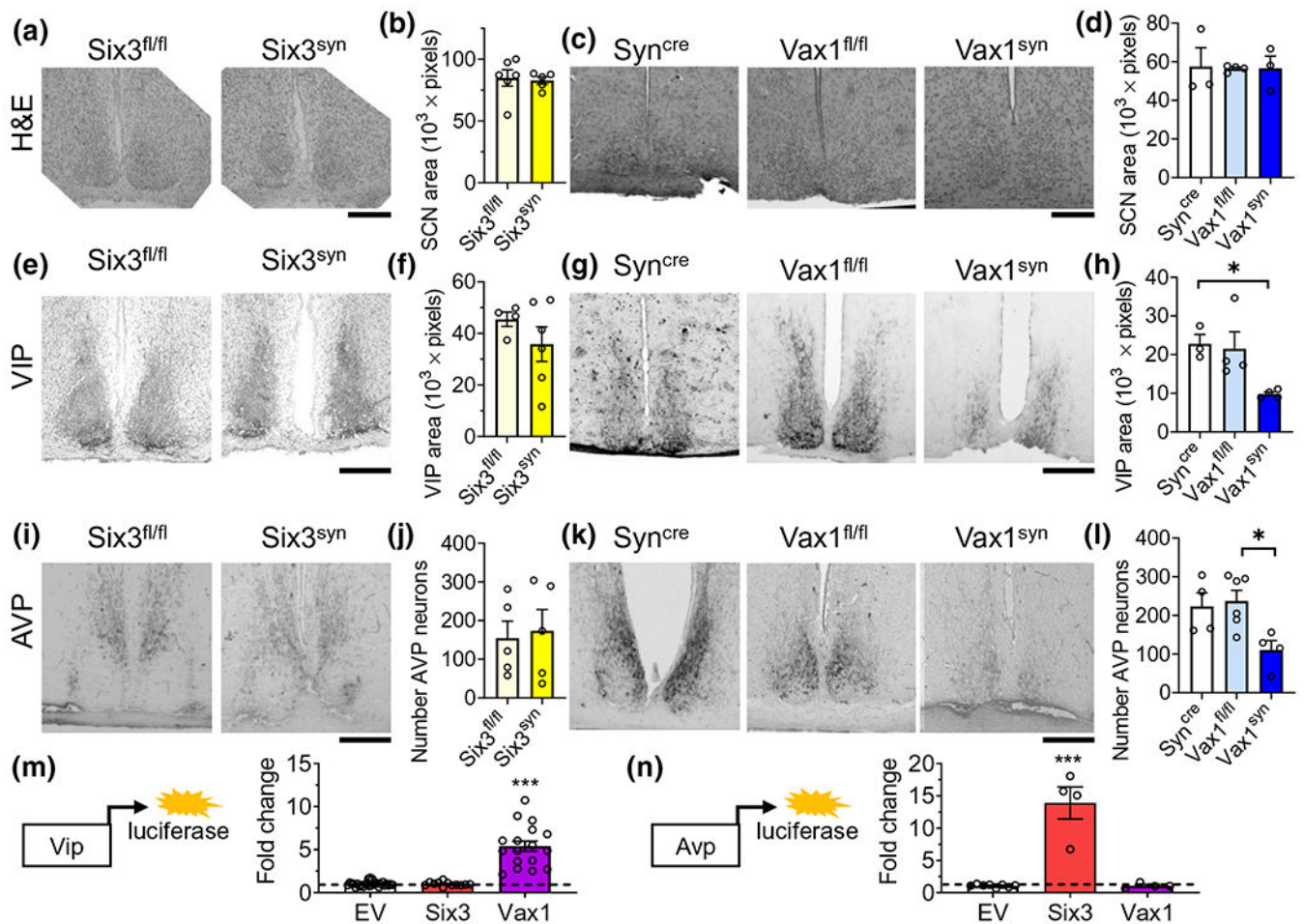
FIGURE 5.

VAX1, but not SIX3, alters VIP and AVP neuropeptide expression in the SCN. Illustrative coronal images and quantification of (a–d) H&E, and immunohistochemistry of (e–h) VIP and (i–l), AVP in adult SCN of *Syn^cre^*, *Six3^fl/fl^*, *Vax1^fl/fl^*, *Six3^syn^*, and *Vax1^syn^* mice. Scale bar 100 μm. All H&E and immunohistochemistry experiments were done in three to six male and female brains per genotype. (b,d,f,h,j,l) Data are represented as average ± *SEM*. *T* test or one-way ANOVA. *, $p < 0.05$. Transient transfection of NIH3T3 cells with (m) *Vip-luciferase* plasmid reporter and (n) *Avp-luciferase* with or without *Six3* overexpression vector, *Vax1* overexpression vector, or empty vector (EV) plasmids. Data are expressed as fold change from EV. $N = 4$–8 independent experiments in duplicate or triplicate. One-way ANOVA as compared to EV; ***$p < 0.001$
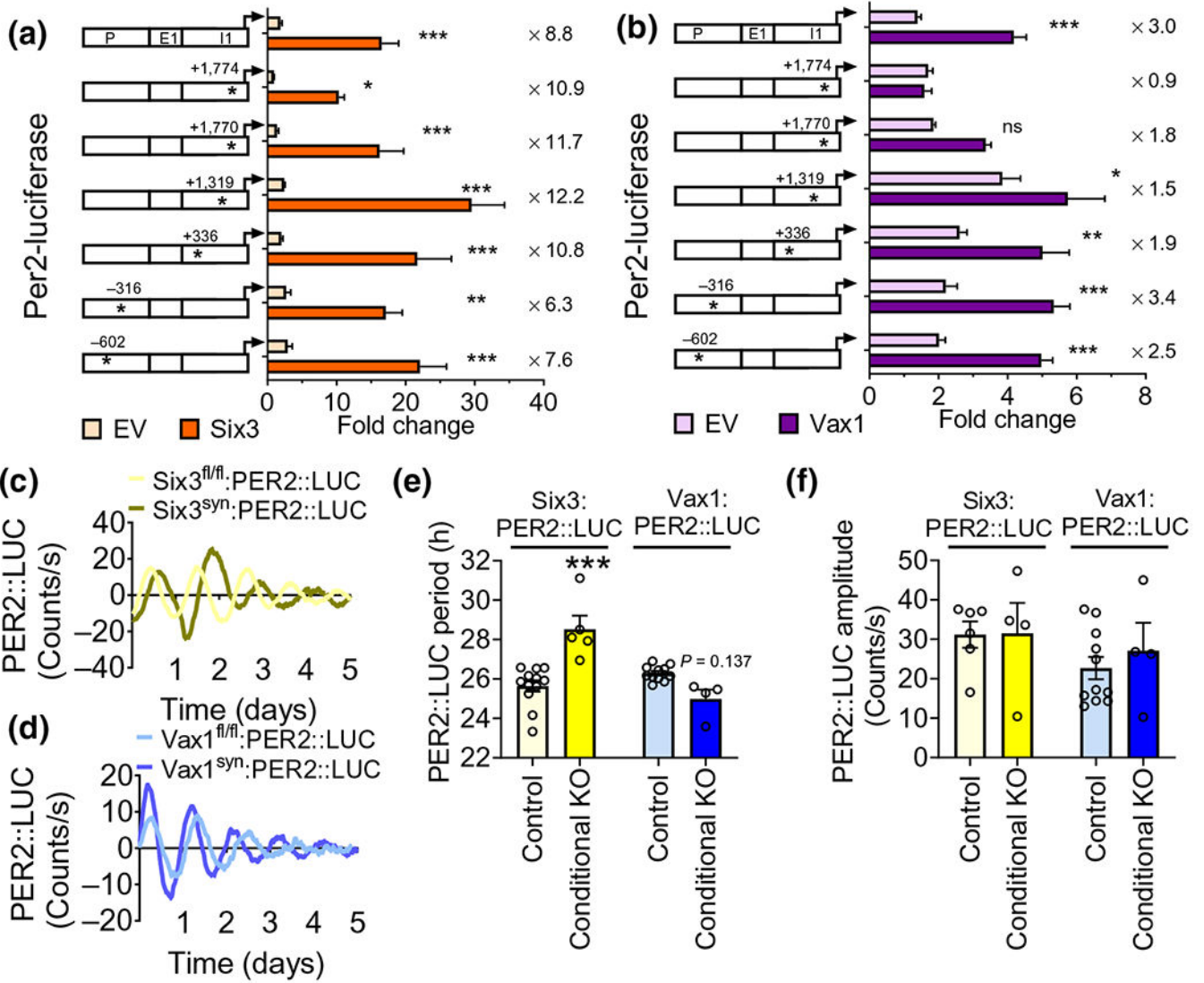
FIGURE 6.

SIX3 and VAX1 regulate Per2 expression in NIH3T3 cells and circadian period in SCN explants. (a,b) Transient transfections of NIH3T3 cells with the mouse *Per2* regulatory region driving luciferase (*Per2*-luciferase) with and without *Six3* overexpression vector (200 ng) or its empty vector (EV, psg5 200 ng), or *Vax1* overexpression vector (20 ng) or its empty vector (EV, pCMV6 20 ng). P is the promoter, E1 is the first exon, and I1 is the first intron for the mouse *Per2* gene. Numbers indicated with the stars on the regulatory regions refer to ATTA sites that have been mutated (see Table 1). Statistical analysis by two-way ANOVA mixed effect model, *$p < 0.05$; **$p < 0.01$; ***$p < 0.001$, $n = 4$–8 in triplicate. (c–f) PER2::LUC recordings in a LumiCycle of *ex vivo* SCN obtained from (c), *Six3^syn:PER2::LUC* and (d), *Vax1^syn:PER2::LUC* diestrus/metestrus females. (e) Histogram of PER2::LUC circadian period of SCN from diestrus/metestrus females. (f) Histogram of PER2::LUC amplitude of SCN from diestrus/metestrus females. Statistical analysis by two-way ANOVA mixed effect model, ***$p < 0.001$, $n = 4$–8
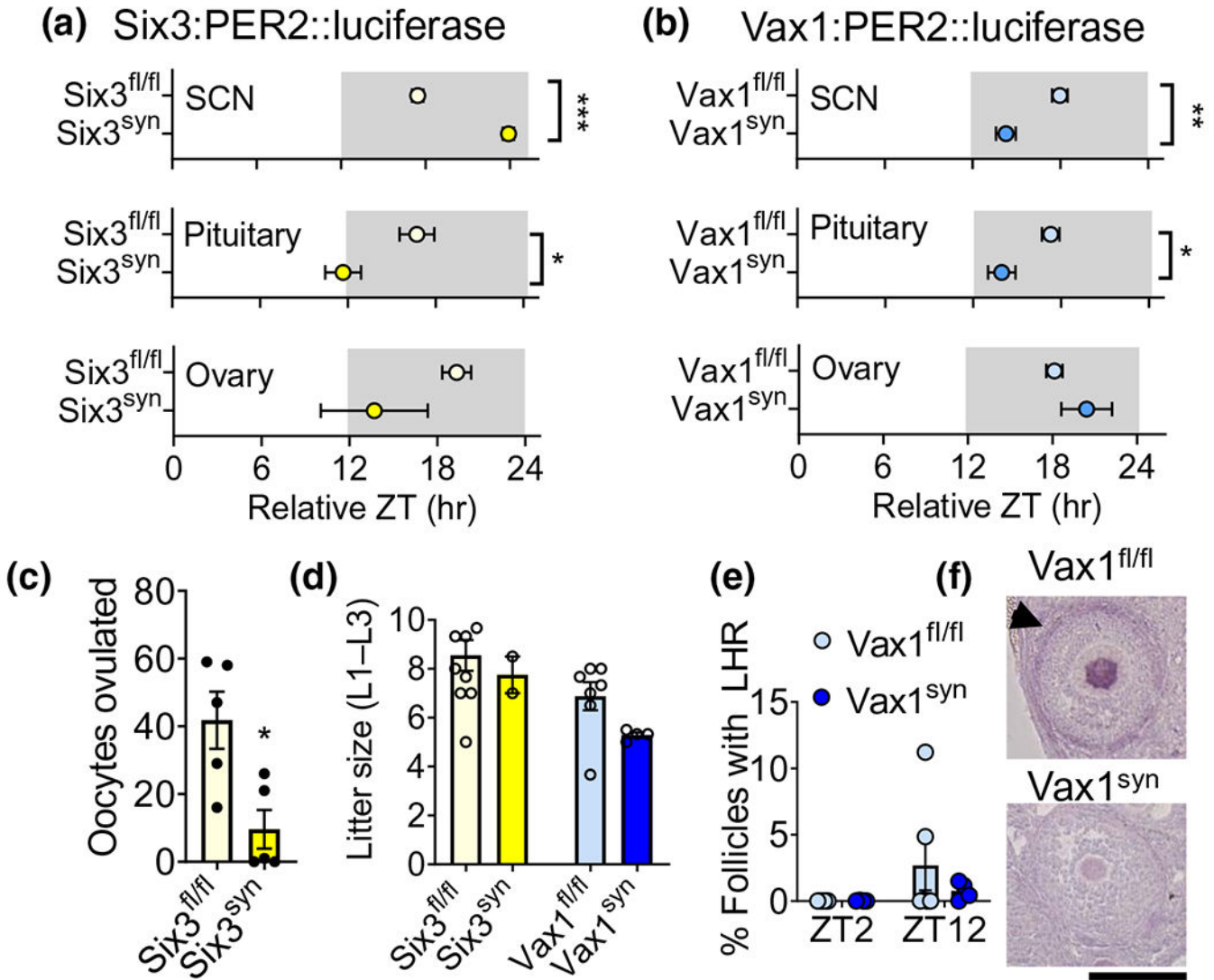
FIGURE 7.

Mistimed PER2::LUC expression in the SCN and pituitary is associated with reduced ovulatory efficiency in $Six3^{syn}$ females. (a,b) PER2::LUC phase (time of first peak) in the SCN, pituitary, and ovary of $Six3^{syn}$:PER::LUC and $Vax1^{syn}$:PER2::LUC diestrus/metestrus females. Data were analyzed by circular analysis of variance high concentration F-test, where * indicates significantly different phases, $n = 3$–19. (c) Oocytes collected in the fallopian tubes after superovulation. Student's t test, $*p < 0.05$, $n = 5$. (d) Average litter size of the first three litters generated by $Six3^{syn}$ females paired with $Six3^{fl/fl}$ males and $Vax1^{syn}$ females paired with $Vax1^{fl/fl}$ males for 4 months. Statistical analysis by one-way ANOVA, $n = 4$–8. (e) Quantification of % follicles with positive LH receptor (LHR) immunohistochemistry staining in ovaries collected at ZT2 and ZT12 in diestrus/metestrus $Vax1^{fl/fl}$ and $Vax1^{syn}$ females ($n = 3$–6), and (f), corresponding illustrative images at ZT12. Black arrow indicates positive staining in theca cells, scale bar 500 μm

Author Manuscript

Author Manuscript

Author Manuscript

Author Manuscript

TABLE 1

Primers used for site-directed mutagenesis in the mouse *Per2*-luciferase plasmid

Position	Mutation	Sequence
−717	TAAT to GCCG	CCTGTAAGGTGCCGAAACTACACCACCG
−602	ATTA to CGGC	CTGCACGGCACGGCTGACCTTATTTCCTG
−316	ATTA to CGGC	GGTCCTTCGGCGGCCCGAGCTGGTC
+366	ATTA to GCCG	GGTCGGAGAGGCCGGTTAGGCATCTTG
+1,319	TAAT to CGGC	TCCTTTATTTCGGCGGTAGCTGTACAGTG
+1,774	TAAT to CGGC	GAGCCTATTACGGCGGGTATAATTTCCTCCAATCTCAG

Note: Table of primers used to mutate ATTA sites within the *Per2* promoter plasmid. Position refers to the number of base pairs from the transcription start site. Underlined sequences indicate mutated bases. All primers were designed using NEBase Changer.

TABLE 2

Reproductive parameters in *Six3^syn* mice

	Six3^flox/flox (Avg ± SEM)	Six3^syn (Avg ± SEM)	p
Age at VO (days) female	24.1 ± 0.3	32.0 ± 1.9	$N = 7$–9, $p = 0.0003$ (***)
Weight at VO (g) female	11.46 ± 0.91	10.77 ± 0.6	$N = 7$–9, $p = 0.56$
PPS (days) male	27.7 ± 1.5	29.9 ± 1.0	$N = 3$–8, $p = 0.27$
Intratesticular testosterone (ng/dl) male	11,342 ± 6,012	12,096 ± 11,476	$N = 5$, $p = 0.96$
LH (ng/ml) female	0.52 ± 0.08	1.0 ± 0.23	$n = 9$–12, $p = 0.036$ (*)
FSH (ng/ml) female	3.133 ± 0.51	5.07 ± 1.67	$n > 10$, $p = 0.27$

Note: Pubertal onset was evaluated by vaginal opening (VO) in females and preputial separation (PPS) in males. Circulating LH and FSH levels of adult *Six3^syn* diestrus/metestrus females. Intratesticular testosterone was measured in adult males. Statistical analysis by Student's *t* test,

*
$p < 0.05$;

***
$p < 0.001$.

TABLE 3

Reproductive parameters in *Vax1^syn* mice

	Vax1^flox/flox (Avg ± SEM)	Vax1^syn (Avg ± SEM)	p
Age at VO (days) female	31.4 ± 2.4	36.8 ± 3.4	n = 5, p = 0.2
Age at PPS (days) male	29.83 ± 0.4	31 (n = 1)	N = 1–6[a]
Circulating testosterone (ng/dl) male	198.1 ± 80.45	39.84 ± 7.76	n = 5–13, p = 0.25
LH (ng/ml) female	0.25 ± 0.04	0.33 ± 0.07	n > 10, p = 0.32
FSH (ng/ml) female	1.23 ± 0.14	0.94 ± 0.14	n > 10, p = 0.15

Note: Pubertal onset was evaluated by vaginal opening (VO) in females and preputial separation (PPS) in males. Circulating hormone levels of adult *Vax1^syn* diestrus/metestrus females. Statistical analysis by Student's *t* test.

[a] No statistical analysis was done due to low *n*.

TABLE 4

Circadian parameters in $Six3^{syn}$ female mice

	LD12:12		DD		Interaction (p)	Light main effect (p)	Genotype main effect (p)
	$Six3^{fl/fl}$ ($n = 8$) Avg ± SEM	$Six3^{syn}$ ($n = 13$) Avg ± SEM	$Six3^{fl/fl}$ ($n = 8$) Avg ± SEM	$Six3^{syn}$ ($n = 13$) Avg ± SEM			
Period (hr)	23.98 ± 0.02	24.01 ± 0.01	23.63 ± 0.11	23.66 ± 0.10	$F(1,19) = 0.14$ ($p = 0.71$)	**$F(1,19) = 7.93$ ($p = 0.01$)**	$F(1,19) = 0.001$ ($p = 0.98$)
Alpha (hr)	11.43 ± 0.34	12.05 ± 0.39	12.05 ± 0.80	10.94 ± 0.61	$F(1,19) = 3.02$ ($p = 0.10$)	$F(1,19) = 0.64$ ($p = 0.43$)	$F(1,19) = 0.74$ ($p = 0.40$)
χ^2 amplitude (Qp)	2,590.35 ± 332.03	195.19 ± 158.17	2,683.01 ± 270.66	991.54 ± 160.62	**$F(1,19) = 7.21$ ($p = 0.01$)**	$F(1,19) = 16.22$ ($p = 0.0003$)	$F(1,19) = 10.78$ ($p = 0.004$)
Activity profile amplitude	N/A	N/A	96.62 ± 24.75	33.09 ± 16.17	N/A	N/A	**$t(16) = 2.15$ ($p = 0.047$)**

Note: Analysis of circadian parameters of $Six3^{fl/fl}$ and $Six3^{syn}$ females on running wheels. Wheel-running behavior was analyzed in LD12:12 and constant darkness (DD), with mean and standard error (*SEM*). Period, alpha, and χ^2 amplitude were analyzed via two-way repeated measures ANOVA and activity profile amplitude was analyzed via t test. Bolded values indicate significant differences, $p < 0.05$.

TABLE 5

Circadian parameters in $Vax1^{syn}$ female mice

	LD12:12		DD		Interaction (p)	Light main effect (p)	Genotype main effect (P)
	$Vax1^{fl/fl}$ ($n = 7$) Avg $\pm$ SEM	$Vax1^{syn}$ ($n = 10$) Avg $\pm$ SEM	$Vax1^{fl/fl}$ ($n = 7$) Avg $\pm$ SEM	$Vax1^{syn}$ ($n = 10$) Avg $\pm$ SEM			
Period (hr)	23.99 ± 0.01	24.00 ± 0.00	23.55 hr ± 0.03	23.64 hr ± 0.06	$F(1,15) = 1.62$ ($p = 0.22$)	$F(1,15) = 12.2$ ($p = 0.003$)	$F(1,15) = 1.00$ ($p = 0.33$)
Alpha (hr)	11.26 ± 0.56	12.18 ± 0.22	11.00 hr ± 0.52	12.56 hr ± 0.61	$F(1,15) = 0.64$ ($p = 0.44$)	$F(1,15) = 0.005$ ($p = 0.94$)	$F(1,15) = 4.12$ ($p = 0.06$)
χ^2 amplitude (Qp)	$2{,}902.82 \pm 532.99$	$2{,}971.97 \pm 309.29$	$3{,}573.05 \pm 363.54$	$2{,}300.46 \pm 296.94$	**$F(1,15) = 8.176$ ($p = 0.01$)**	$F(1,15) = 7.49\text{e-}006$ ($p = 1.0$)	$F(1,15) = 1.643$ ($p = 0.22$)
Activity profile amplitude	N/A	N/A	95.9 ± 15.73	143.3 ± 22.82	N/A	N/A	$t(15) = 1.77$ ($p = 0.097$)

Note: Analysis of circadian parameters of $Vax1^{fl/fl}$ and $Vax1^{syn}$ females on running wheels. Wheel-running behavior was analyzed in LD12:12 and constant darkness (DD), with mean and standard error (SEM). Period, alpha, and χ^2 amplitude were analyzed via two-way repeated measures ANOVA and activity profile amplitude was analyzed via a t test. Bolded values indicate significant differences, $p < 0.05$.